Applied Catalysis B: Environmental 123–124 (2012) 52–68

Contents lists available at SciVerse ScienceDirect

Applied Catalysis B: Environmental

journal homepage: www.elsevier.com/locate/apcatb

Review

Graphene as a new carbon support for low-temperature fuel cell catalysts

Ermete Antolini*

Scuola di Scienza dei Materiali, Via 25 aprile 22, 16016 Cogoleto, Genova, Italy

ARTICLE INFO

Article history:
Received 7 December 2011
Received in revised form 23 March 2012
Accepted 17 April 2012
Available online 24 April 2012

Keywords:
Fuel cells
Catalyst supports
Graphene
Platinum

ABSTRACT

Highly dispersed catalysts on a conductive support, commonly platinum and platinum-based catalysts, are used as electrode materials in low-temperature fuel cells. Carbon blacks are commonly used as fuel cell catalysts supports, but their properties are not completely satisfactory. Thus, in the last years carbon black alternative materials such as nanostructured carbons, ceramic and polymer materials have been proposed as fuel cell catalyst supports. Very recently, in consideration of their high surface area, high conductivity, unique graphitized basal plane structure and potential low manufacturing cost, graphene nanosheets have been investigated as a support for low-temperature fuel cell catalysts. This paper presents an overview of graphene nanosheets used as supports for fuel cell catalysts. In particular, the catalytic activity and durability of catalysts supported on graphene are compared with those of catalysts supported on the commonly used carbon blacks and on carbon nanotubes, that is, on rolled graphene.

Contents

1. Introduction

Graphene is a two-dimensional one-atom-thick planar sheet of sp^2 bonded carbon atoms, having a thickness of 0.34 nm, which is considered as the fundamental foundation for all fullerene allotropic dimensionalities [1,2]. As can be seen in Fig. 1 [3], in addition to its planar state, graphene can be wrapped into zero-dimensional spherical buckyballs, rolled into one-dimensional carbon nanotube (CNT), or stacked into three-dimensional graphite [1–3]. A variation on graphene are nano-platelets, which consist of small stacks of graphene that are 1–15 nm thick. Since graphene was discovered [1,4,5], it has attracted great interest from both fundamental science and applied research [6].

Recently, graphene nanosheets (GNS) have been investigated as a support for low-temperature fuel cell catalysts. Highly dispersed metal catalysts, commonly platinum or platinum-based catalysts, on a conductive support, commonly carbon blacks, are used as electrode materials for oxidation and reduction reactions in fuel cells fuelled with hydrogen (polymer electrolyte fuel cells, PEMFCs) or small organic molecules such as methanol (direct methanol fuel cells, DMFCs), ethanol (direct ethanol fuel cells, DEFCs), formic acid (direct formic acid fuel cells, DFAFCs) and glycerol (direct glycerol fuel cells, DGlyFCs) [7]. In such catalysts, the high surface to volume ratio of metal particles maximizes the area of the surface available

* Tel.: +39 010 918 2880; fax: +39 010 918 2368.
E-mail addresses: ermantol@libero.it, ermete@iqsc.usp.br

0926-3373/$ – see front matter © 2012 Elsevier B.V. All rights reserved.
http://dx.doi.org/10.1016/j.apcatb.2012.04.022

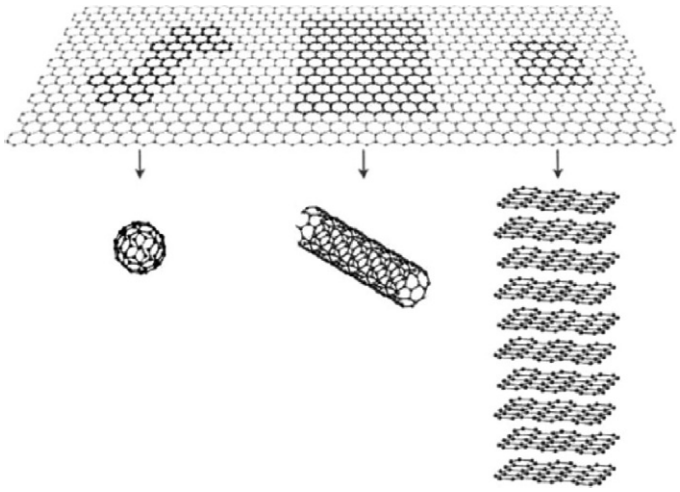

Fig. 1. Schematic representation of graphene, which is the fundamental starting material for a variety of fullerene materials: buckyballs, carbon nanotubes, and graphite.
Reproduced from Ref. [3], copyright 2011, with permission from Elsevier.

for the reactions. The structure and proper dispersal of these metal particles make low-loading catalysts feasible for fuel cell operation, lowering the cost of the system. The main requirements of a suitable fuel cell catalyst support are (i) high surface area, to obtain high metal dispersion, (ii) suitable porosity, to boost gas flow, (iii) high electrical conductivity, and (iv) high stability under fuel cell operational conditions [8]. Carbon nanotubes were the most investigated carbon nanostructures as carbon black alternative catalyst support for low temperature fuel cells [8]. The high crystallinity of CNTs make these materials highly conductive, the high surface area and high amount of mesopores result in a high metal dispersion and a good reactant flux in tubular structure. Moreover, CNTs have a positive effect on the catalyst structure. All these characteristics of CNTs result in a higher catalytic activity and a higher stability of catalysts supported on CNTs than those supported on carbon blacks [8]. A problem for the commercialization of carbon nanotubes is their higher cost compared to that of carbon blacks. The combination of the high surface area (theoretical value of 2630 $m^2 g^{-1}$) [9], high conductivity [1], unique graphitized basal plane structure and potential low manufacturing cost [9,10] makes graphene sheets a promising candidate as low-temperature fuel cell catalyst support. In comparison with CNTs, graphene not only possesses similar stable physical properties but also larger surface area. Additionally, production cost of GNS in large quantities is much lower than that of CNTs. Thus, fuel cell catalysts supported on GNS have been synthesized and characterized, their electrocatalytic activity and durability have been evaluated by half-cell measurements and tests in single fuel cells have also been performed. To increase catalyst dispersion, modified-graphene with epoxy, hydroxyl and carboxyl groups (f-GNS), poly(diallyldimethylammonium chloride) (PDDA–GNS) and nitrogen (N–GNS) have been largely investigated as catalyst supports. To improve the characteristics of graphene nanosheets, composite graphene–carbon fibers (GNS–CF) graphene–carbon nanotubes (GNS–CNT), graphene–polypyrrole (GNS–PPy) and graphene–tin oxide (GNS–SnO_2) materials have also been tested as metal supports. In recent reviews of graphene in energy conversion and storage, sections were devoted to applications of graphene in fuel cell components [3,11,12]. In our previous work [8], an overview of carbon supports for low-temperature fuel cell catalysts has been presented, with particular attention on new carbon materials. As the use of graphene as fuel cell catalyst support started about in 2009, that is, after the preparation of the over-mentioned review, this material has not been considered. So, to complete the picture, in this work the use of graphene as support for fuel cell catalysts is reviewed, and, in particular, the catalytic activity and durability of catalysts supported on graphene are compared with those of catalysts supported on the commonly used carbon blacks and on carbon nanotubes, that is, on rolled graphene.

2. Synthesis of GNS and GNS-supported catalysts (Me/GNS, Me = mono or bimetallic catalysts)

2.1. Synthesis of GNS

The first graphene sheets were obtained by extracting monolayer sheets from the three-dimensional graphite using a technique called micromechanical cleavage in 2004 [4]. Then, many works efforts have been addressed to the treatment of graphite and production of monolayer graphene sheets, as reported in excellent reviews [6,13]. Graphene can be synthesised without the formation of graphene oxide (GO) by different methods, such as epitaxial growth by ultra high vacuum graphitization [14], chemical vapor deposition [15], solvothermal synthesis with pyrolysis [16] and electrochemical methods [17–20]. The most commonly method to obtain GNS, however, is to oxidise graphite to graphene oxide, followed by exfoliation and reduction of GO to GNS. GO consists of graphene oxide sheets having their basal planes decorated mostly with epoxide and hydroxyl groups, in addition to carbonyl and carboxyl groups located presumably at the edges [21–23]. These oxygen functionalities render the graphene oxide layers hydrophilic and water molecules can readily intercalate into the interlayer galleries. GO can therefore be also thought of as a graphite-type intercalation compound with both covalently bound oxygen and non-covalently bound water between the carbon layers. GO is produced by the oxidative treatment of graphite via one of three principal methods developed by Brodie [24], Staudenmaier [25] and Hummers and Offeman [26], respectively. Each method is based on the oxidation of graphite in concentrated strong mineral acid with strong oxidizing agents. GO directly exfoliated in water due to its hydrophilic property [27]. Then, GO is chemically or electrochemically reduced to GNS. GO can be reduced to GNS by $NaBH_4$ [28], hydroquinone [28] and hydrogen sulphide [29]. Stankovich et al. [30] investigated the chemical reduction of exfoliated graphene oxide sheets with several reducing agents and found hydrazine hydrate ($H_2NNH_2{\cdot}H_2O$) to be the best one in producing very thin graphene-like sheets. SEM images revealed that the reduced GO material consists of randomly aggregated, thin, crumpled sheets closely associated with each other and forming a disordered solid (Fig. 2a). The folded regions of the sheets (Fig. 2b) were found to have average widths of ~2 nm by high-resolution SEM. Surface area measurement of the reduced GO sheets via nitrogen gas absorption yielded a BET value of 466 $m^2 g^{-1}$. This high specific surface area is an indication of the degree of GO exfoliation prior to the reduction. However, it is still lower than the theoretical specific surface area for completely exfoliated and isolated graphene sheets. According to Saner et al. [31], the best method for the production of mostly exfoliated (minimum number of layers) graphene nanosheets is the oxidation of the sonicated graphite flake, ultrasonic treatment of GO, and chemical reduction of sonicated GO samples. This procedure reduces the average number of graphene sheets from 86 in the raw graphite to 9 in GNS. Electrochemical reduction of graphene oxide was also carried out by electrochemical methods [32–34].

Functionalized GNS by surface epoxy, hydroxyl and carboxyl groups were synthesized through simple synthesis processes. These processes include the chemical oxidation of common

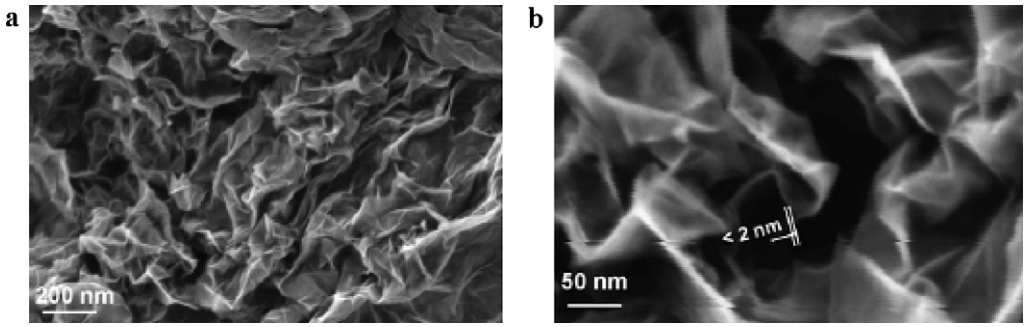

Fig. 2. (a) SEM image of aggregated reduced GO sheets. (b) A platelet having an upper bound thickness at a fold of ~2 nm.
Reproduced from Ref. [30], copyright 2007, with permission from Elsevier.

graphite to graphite oxide and the subsequent thermal exfoliation of the GO to GNS [35,36]. Rapid heating of GO results in its expansion and delamination caused by rapid evaporation of the intercalated water and evolution of gases produced by thermal pyrolysis of the oxygen-containing functional groups. Such thermal treatment has recently been suggested to be capable of producing individual functionalized graphene sheets [35,36]. Fig. 3 shows an illustration of the synthetic route used to obtain the GNSs and their SEM images [37]. The SEM image of graphite shows a bulky and spherical shape. After the chemical oxidation and thermal exfoliation, GO and GNSs present a sheet-like morphology. C1s XPS results (Table 1) revealed the formation of surface functional groups on the obtained materials; the spectra contain four resolved peaks corresponding to the sp^2-hybridized C–C and oxygenated functional groups (C–OH, C–O–C, and HO–C=O). The relative C–C peak area in the GO was significantly reduced, while the peaks associated with oxidized carbon increased, implying that a chemical oxidation process of graphite occurred. The total fraction of oxygenated functional groups on the GNSs (37.1%) was between those of graphite (32.0%) and GO (67.1%), showing that the GNSs were moderately functionalized with these species.

Table 1
Binding energy and relative area of carbon–carbon and oxygenated functional groups for graphite, GO and GNSs.

	C–C	C–OH	C–O–C	HO–C=O
Graphite				
Binding energy (eV)	284.5	285.1	286.7	288.7
Relative area (%)	68	23.2	6.3	2.5
GO				
Binding energy (eV)	284.5	285.0	286.6	288.1
Relative area (%)	32.9	29.1	25.2	12.8
GNS				
Binding energy (eV)	284.5	285.4	286.4	288.9
Relative area (%)	62.9	13.7	18.8	4.6

Reproduced from Ref. [37], copyright 2011, with permission from Elsevier.

The reduced graphene sheets, however, tend to form irreversible agglomerates because of the van der Waals interaction and even restack to form graphite in the reduction from GO suspension solution or drying process [38], leading to a loss of its ultrahigh surface area. Si and Samulski [39] report a metal nanoparticle–graphene composite with a partially exfoliated graphene morphology derived from drying aqueous dispersions of

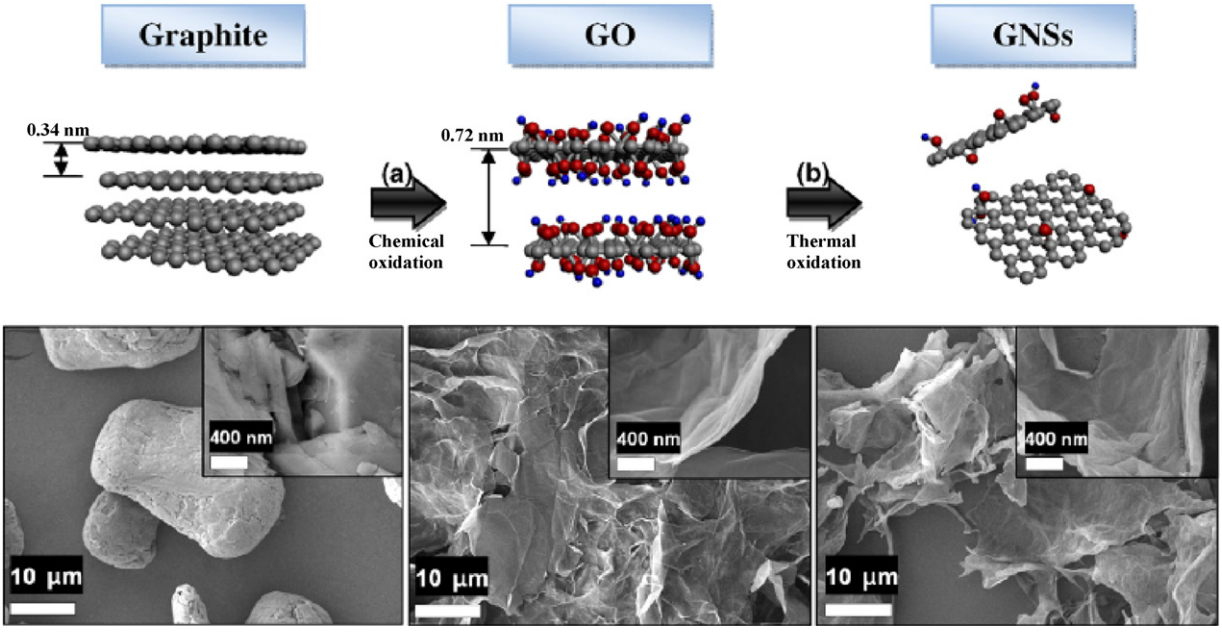

Fig. 3. Illustration of graphene synthesis from graphite and their hypothetical structure images together with SEM pictures (insets are high resolution images). (a) Chemical oxidation to form GO from graphite. (b) Thermal exfoliation to synthesize surface functionalized GNSs from GO. The red and blue colored atoms on the surface of graphite oxide and GNSs represent oxygen and hydrogen species, respectively. (For interpretation of the references to color in this figure legend, the reader is referred to the web version of the article.)
Reproduced from Ref. [37], copyright 2011, with permission from Elsevier.

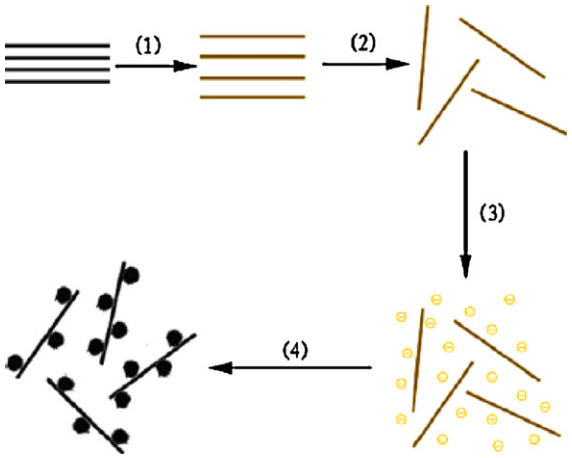

Fig. 4. The route to synthesize of Pt/graphene nanocomposites. (1) Oxidation of graphite to graphite oxide (GO); (2) exfoliation of graphite oxide in water by sonication; (3) addition of Pt ions to GO solution; and (4) chemical reduction of GO and Pt ions leading to the formation of Pt/graphene composites.
Reproduced from Ref. [46], copyright 2009, with permission from Elsevier.

platinum nanoparticles adhered to graphene. Face-to-face aggregation of graphene sheets is arrested by 3–4 nm size Pt crystallites on the graphene surfaces, and in the resulting jammed Pt–graphene composite the Pt acts as spacers resulting in mechanically exfoliated, high-surface-area material. Moreover, Pt nanoparticles play a reductive or catalytic role during the reduction process of GO [40]. These works opened the way to studies on the use of graphene-supported platinum catalysts for low-temperature fuel cells.

2.2. Synthesis of Me/GNS

There are essentially two-way to prepare Me/GNS, that is, (1) simultaneous and (2) sequential reduction of GO and metal precursors. It has been reported that metallic nanoparticles not only play an essential role in catalytic reduction of graphene oxide, but also prevent the aggregation and restacking of the reduced graphene oxide by the formation of graphene particle composites [38,39]. Thus, generally, metal precursors are deposited on GO and then are reduced simultaneously by different methods such as ethylene glycol reduction method [38,40–45], $NaBH_4$ reduction method [46,47], PVP/hydrazine reduction method [48], sodium citrate reduction method [49,50] microwave heating method [51], microwave polyol synthesis [52–55] and colloidal method [56]. A general scheme illustrating the synthesis of Pt/graphene nanocomposites is shown in Fig. 4 [46]. Pt/GNS, prepared by synchronous reduction of H_2PtCl_6 and GO suspension using $NaBH_4$ [47], tended to form a stack of graphitic structure when the suspension was dried by conventional evaporation of water in the suspension. Also if Pt can act as spacers for graphenes, leading to a potential high-surface-area material, however, the aggregation of Pt/GNS was still severe. Lyophilization was introduced to prevent the restack of these sheets during liquid water departure in the conventional drying process. The water in the suspension can be sublimated from solid ice to gas, preventing accumulation of Pt/GNS [47].

The latter method is based on the separate reduction of GO, followed by the deposition and reduction of metal precursors on reduced GO [57–59]. However, it is very difficult to deposit metal nanoparticles on the hydrophobic GNS without surface functionalization. Thus, the sequential method is overall used to prepare catalysts supported on functionalized graphene with either epoxy, hydroxyl and carboxyl groups (f-GNS) [37,60–64] or poly(diallyldimethylammonium chloride) (PDDA–GNS) [65,66].

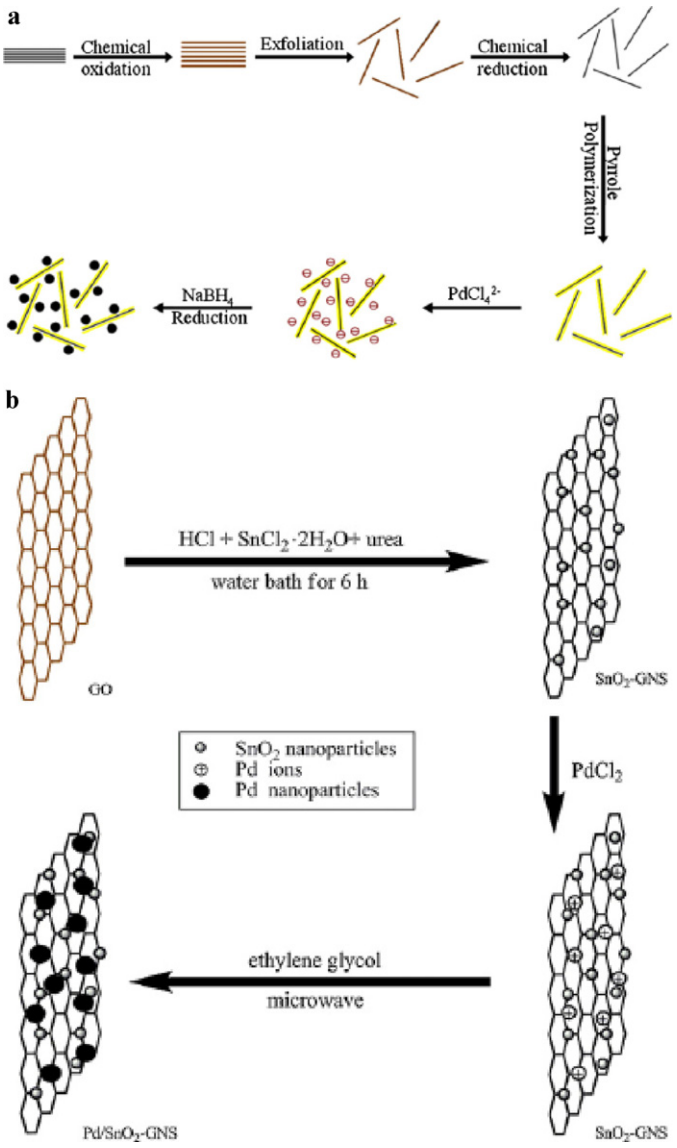

Fig. 5. Schematic representation of the synthesis of (a) Pd/PPy–GNS and (b) Pd/SnO_2–GNS catalysts.
Reproduced from Ref. [72], copyright 2011, and Ref. [75], copyright 2010, with permission from Elsevier.

Two original and interesting sequential green synthesis methods of Me/GNS consist (1) in the electrochemical reduction of GO, followed by the electrochemical deposition and reduction of Pt precursor [67], and (2) in the photocatalytic reduction of GO using a phosphotungstate as a homogeneous photocatalyst under UV irradiation, followed by the injection of Ag, Au, and Pd precursors on the graphene surface [68]. A self-assembly method was used to synthesize high-density Pt nanoparticles on chemically reduced graphene sheets [69]. By employing 1-pyrenemethylamine ($Py\text{-}CH_2NH_2$) as the interlinker to form a self-assembled layer on the surface of graphene nanosheets, high-density Pt nanoparticles on GNS were obtained. Electroless deposition has been successfully utilized as a versatile platform for the synthesis of GNS-supported Me catalysts [70], by taking advantage of the redox potential differences between substrates (Cu or Zn) and the metal ions (Me^{m+}/Me), and the excellent conductivity of GNS.

Finally, an inverse sequential method, based on the deposition of metal precursor on partially reduced GO and separate reduction

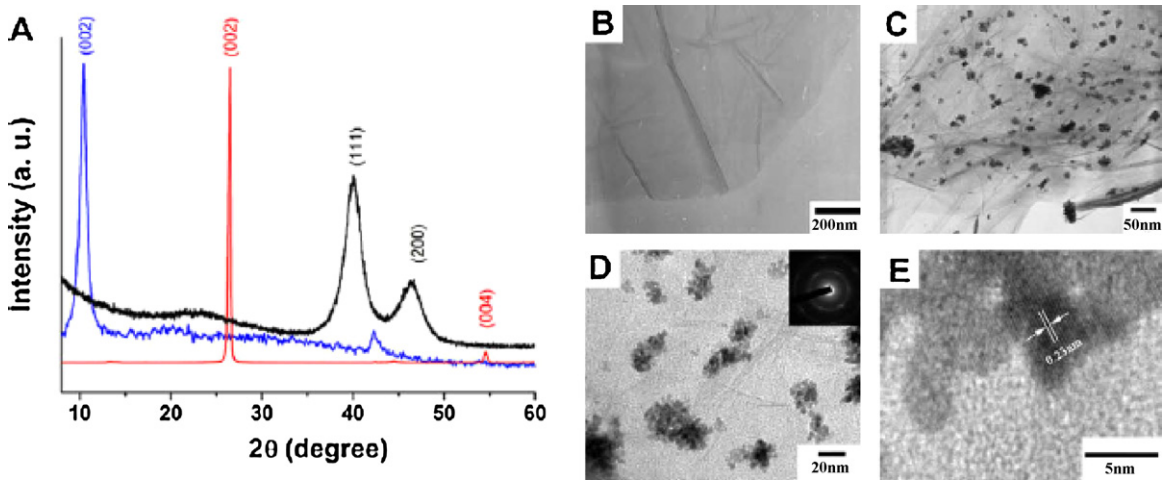

Fig. 6. XRD patterns (A) of graphite (red line, bottom), graphite oxide (blue line, middle) and Pt/graphene (black line, top); TEM images of GO (B); Pt/graphene composites at different magnification (C) and (D), inset of (D): SAED of Pt/graphene; HRTEM images of Pt/graphene (E). (For interpretation of the references to color in this figure legend, the reader is referred to the web version of this article.)

Reproduced from Ref. [46], copyright 2009, with permission from Elsevier.

of the metal, followed by the complete reduction of GO, has been reported [71].

The preparation of Pd supported on hybrid GNS–PPy and GNS–SnO_2 materials has been carried according to the schemes shown in Fig. 5a and b, respectively. First, the hybrid support was prepared, by in situ polymerization of pyrrole to fabricate GNS–PPy nanocomposites [72–74], and by a chemical-solution method to obtain GNS–SnO_2 [75]. Then, the catalyst precursor was deposited and reduced on the composites. Two synthesis methods of GNS–CNT composite materials, instead, have been proposed: a method consists in the preparation of the GNS–CNT composite, by mixing the required amount of GNS and CNT, followed by the deposition and reduction of metal precursor on the composite support [76]. Another preparation method of GNS–CNT is based on the synthesis of a GNS-supported catalyst, followed by the mixing of Me/GNS and CNT [77,78].

3. Structural characterization of GNS- and modified-GNS supported catalysts

The structural characteristics of Pt/GNS prepared by simultaneous reduction of GO and H_2PtCl_6 with $NaBH_4$ are shown in Fig. 6 [46]. The XRD pattern of GO, showing the disappearance of the graphite peak at 2θ about 26.4° and the appearance of a peak at 2θ 10.4°, reveals the successful oxidation of the starting graphite (Fig. 6a). The diffraction peaks at 2θ 39.9° and 46.2° correspond to the (1 1 1), and (2 0 0) facets of platinum crystals. As shown in Fig. 6b, GO was fully exfoliated into nanosheets with micrometer-long wrinkles by ultrasonic treatment, illustrating clearly the flake-like shapes of graphite oxide sheets. The typical TEM image of Pt/graphene nanocomposites (Fig. 6c) illustrated that the "Pt nano clusters" were deposited on the basal planes and the edges of graphene. A further magnification (Fig. 6d) indicated that the "Pt nano clusters" consisted of small Pt nanoparticles with diameter of about 5–6 nm. The selected area electronic diffraction (SAED) shows that the Pt nanoparticles belonged to single crystal. Lattice fringes with a spacing of 0.23 nm were clearly visible in the HRTEM image (Fig. 6e).

The very high surface area of GNS allows to load high amounts of catalysts maintaining a low metal particle size, particularly for functionalized GNS [37,45,56,61,62]. The surface groups on f-GNS may function as anchoring sites for Pt precursor to prevent the aggregation of the Pt nanoparticles. Choi et al. [37] compared Pt particle size of Pt/C and Pt/f-GNS catalysts, prepared by deposition of Pt precursor on the carbon support, followed by reduction with H_2 at 300 °C, for different metal loading. TEM images of the Pt/C and Pt/f-GNS catalysts revealed that for the Pt/f-GNS catalyst the Pt nanoparticles were highly dispersed even up to 80 wt% Pt/f-GNS, as shown in Fig. 7. The Pt particle sizes in the samples of 40, 60, and 80 wt% Pt/f-GNS were ca. 1.8, 2.0, and 2.9 nm, respectively, whereas those of Pt/C catalysts were ca. 1.9, 4.8, and 7.0 nm, respectively (TEM images for the 60 and 80 wt.% Pt/C sample are not displayed). Generally, high metal dispersions on carbon black supports are difficult to obtain, especially with high metal loading, because the metals tend to sinter due to weak interactions between the metal and the carbon. Conversely, the increase in particle size for the Pt/GNS catalysts appeared to be effectively suppressed at 3 nm or smaller, even at Pt loadings as high as 80 wt%. Lee et al. [79] compared the structural characteristics of PtRu supported on graphene nanosheets and multi wall carbon nanotubes (MWCNTs), both prepared by a hydrothermal method. As can be seen in Fig. 8a and b, the PtRu particles were successively dispersed on both

Table 2
Particle size of some GNS-supported catalysts with high metal loading (>50 wt%).

Supported catalyst	Synthesis method	Metal loading/wt%	Particle size/nm	Reference
PtRu/GNS	Simultaneous reduction of GO and metals by colloidal method	80	2.0	[56]
Pt/GNS	Simultaneous reduction by EG reduction method	70	2.9	[45]
Pd/f-GNS	Sequential reduction. Thermal exfoliation/H_2, 300 °C	60	1.8	[61]
Pt/f-GNS		60	1.9	
Pt/f-GNS	Sequential reduction. Thermal exfoliation/H_2, 300 °C	60	1.8	[62]
PtRu/f-GNS		60	2.2	
Pt/f-GNS	Sequential reduction. Thermal exfoliation/H_2, 300 °C	60	2.0	[37]
		80	2.9	

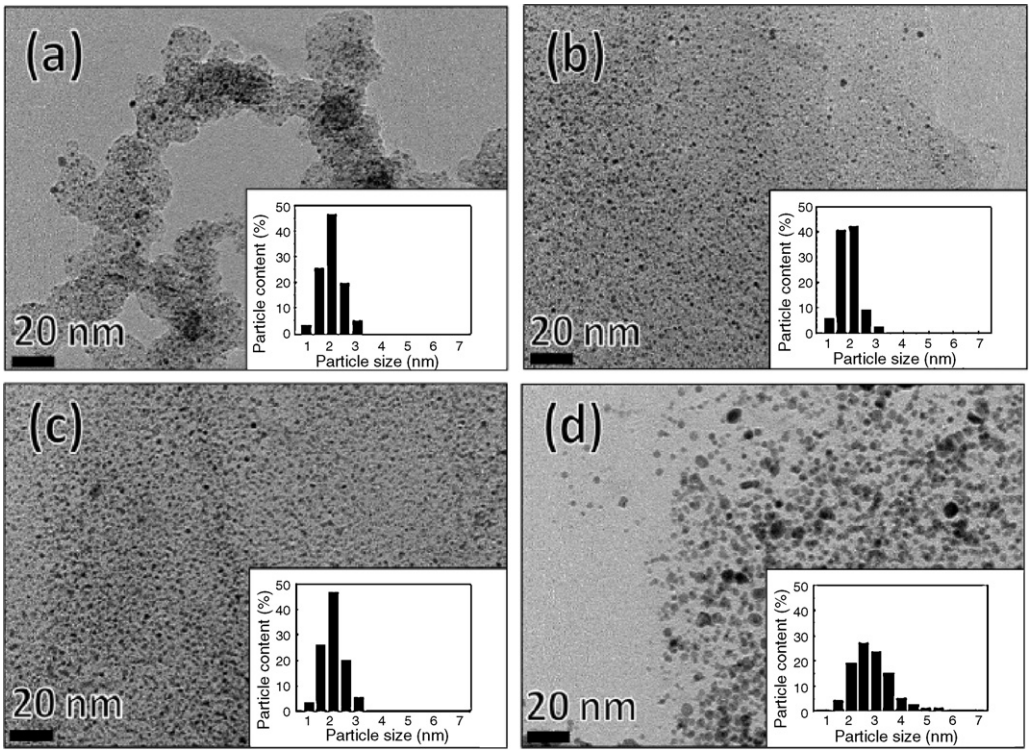

Fig. 7. Representative TEM images of the (a) 40 wt% Pt/C, (b) 40 wt%, (c) 60 wt%, and (d) 80 wt% Pt/GNS catalysts as well as the particle size distributions of the metal nanoparticles.

Reproduced from Ref. [37], copyright 2011, with permission from Elsevier.

specimens. However, PtRu particles were more uniformly dispersed on GNS than on MWCNTs (Fig. 8c and d). Comparing the particle size distributions, the average particle size of PtRu/GNS (2.2 nm) was smaller than PtRu/MWCNT (3.7 nm) (Fig. 8e and f). The difference in particle dispersion and size was explained by the different specific surface area of carbon support materials. The particle size of some GNS-supported catalysts with high metal loading are reported in Table 2.

Yoo et al. [58,80] found that Pt particles below 0.5 nm in size are formed on GNS, which would strongly interact with the support, thus modifying the electronic structure of Pt, and, as a consequence, its catalytic activity. They prepared 20 wt% Pt/GNS and compared the structural characteristics of this catalyst with that of a commercial 20 wt% Pt/C. GNS revealed a curled morphology, consisting of a thin wrinkled paper-like structure as shown by the SEM images in Fig. 9a. The thickness of the GNS was estimated to be between 3 and 7 nm by SEM measurements, corresponding to ca. 10–20 stacked layers of monatomic graphene sheets. In addition, as shown in the TEM images in Fig. 9b, the thin GNS were irregularly bent and deformed like crumpled paper, and the graphene sheets were randomly stacked. As can be seen in Fig. 9c and d, Pt particles with sizes of 2–3 nm for Pt/GNS and Pt/C were well-dispersed on the GNS and the carbon black. Fig. 9e shows the HAADF-STEM image of Pt/GNS: it can be seen that platinum is finely dispersed on the GNS with many clusters being less than 0.5 nm in diameter and with the largest being 2 nm wide. The size of the smaller Pt clusters were estimated to be 0.3 nm. The HAADF-STEM image of Pt/C, instead, did not show any sub-nano-Pt clusters supported on the carbon black (Fig. 9f).

Stacking of 2D individual graphene sheets is effectively inhibited by introducing 1D one-dimensional carbon nanotubes to form a 3D hierarchical structure which enhances the utilization of GNS-based composites. Yang et al. [77] observed the effective inhibition on the face-to-face aggregation of GNS by introducing CNTs as a nanospacer. The hierarchical GNS–CNTs architecture with a 3D graphitic, porous structure possesses synergistic effects on enhancing the specific electrolyte-accessible surface area of composites and the active sites of Pt. From FE-SEM images shown in Fig. 10, the surfaces of all composites exhibit typically crumpled and porous architectures which are different from that of carbon black and graphite. Pt/GNS–CNTs show higher porosity than Pt/GNS, suggesting the successful insertion of CNTs into GNS to enlarge the space between graphene sheets and, as a consequence, to reduce GNS stacking. A porous network structure of a Pt–GNS–MWCNT composite cathode was formed onto a carbon cloth by spray coating from a Pt–GNS and MWCNT dispersion [78]. In addition to the positive effect of CNT avoiding the stacking of GNS, the porous network structure induced by the MWCNTs acted as a pathway for mass transfer of the chemical reactants and products and as an electrical bridge. Fig. 11 shows a schematic diagram of the structures of the Pt–GNS cathode and the Pt/GNS–MWCNT composite cathode.

4. Electrochemical properties of Me/GNS

4.1. Electro-catalytic activity of Me/GNS

To the aim to evaluate their possible use in low-temperature fuel cells, the activity for small organic molecule oxidation and oxygen reduction of catalysts supported on GNS has been compared with that of the same catalysts supported carbon blacks and CNTs. In the following paragraphs the electrocatalytic activity of bare GNS, modified-GNS and hybrid GNS-containing supports, obtained by half-cell measurements, is reviewed.

4.1.1. Me supported on bare GNS

4.1.1.1. Electro-catalytic activity of Me/GNS for alcohol, formic acid, hydrogen and carbon monoxide oxidation. The most part of GNS-supported catalysts has been evaluated for a potential

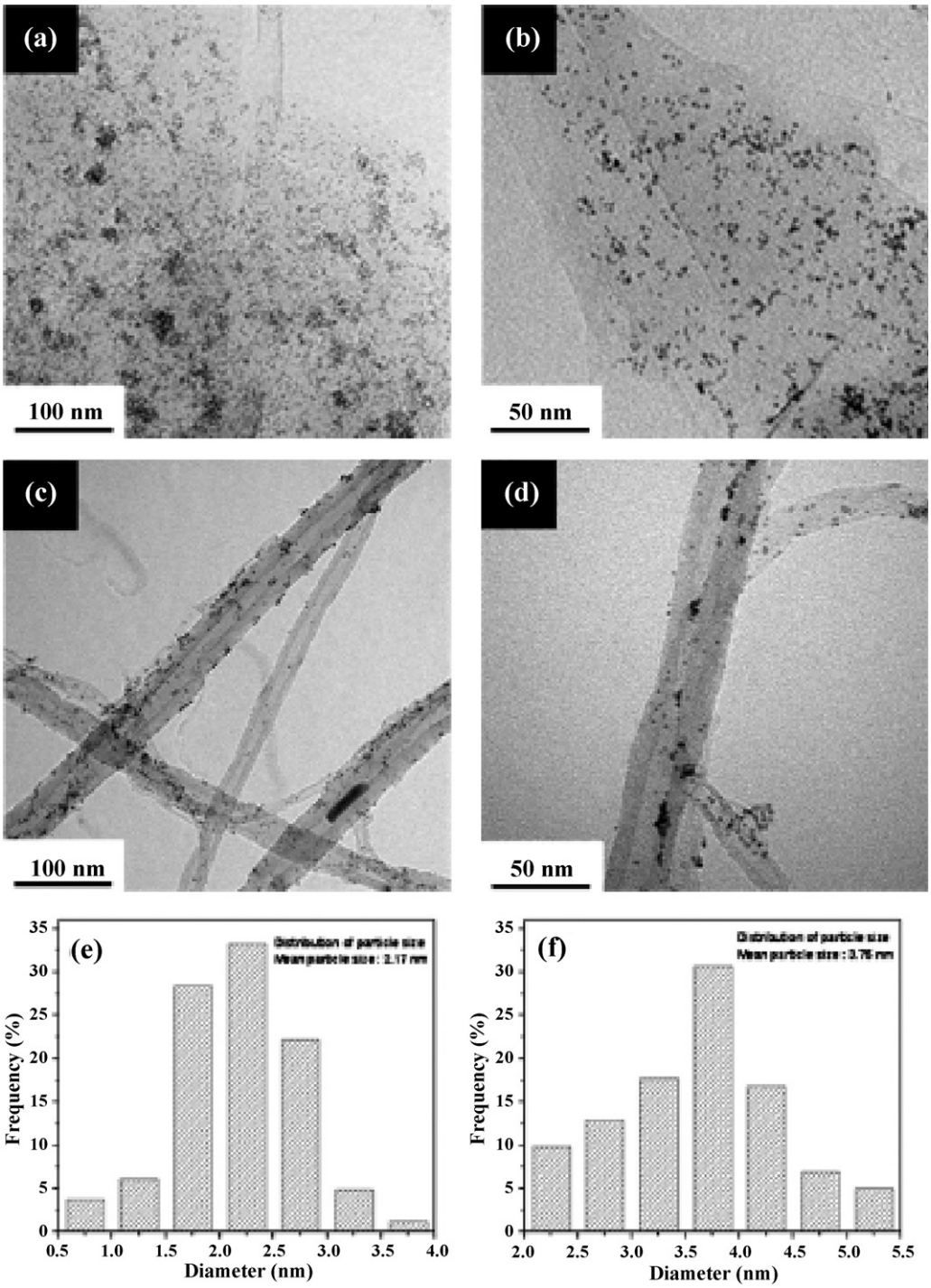

Fig. 8. TEM images of Pt–Ru/graphene (a, b) and Pt–Ru/MWCNTs (c, d) catalysts and size distribution of Pt–Ru nanoparticles in both catalysts (e: graphene sheet, f: MWCNT). Reproduced from Ref. [79], copyright 2011, with permission from Elsevier.

application as anode materials in direct methanol fuel cells [40,41,46–48,52,55,56,67,79–85]. Generally, Pt and Pt-based catalysts supported on graphene nanosheets presented higher catalytic activity for methanol oxidation than that of the same catalysts supported on carbon blacks [41,46–48,55,56,80,82], carbon nanotubes [40,48,79,85] and graphite [41]. For example, the electrocatalytic activity for methanol oxidation of PtNi/GNS, PtNi/C and PtNi/CNT was evaluated by CV measurements (Fig. 12) [48]. The peak current obtained at the PtNi/GNS catalyst (curve a) was much higher than the current obtained at the PtNi/SWCNT (curve b) and PtNi/C (curve c) catalysts. Moreover, the starting potential for methanol oxidation at the PtNi/GNS catalyst is about 110 mV, which is 100 mV more negative than the potential at the PtNi/SWCNT or PtNi/C catalysts (inset of Fig. 12), indicating that graphene has a significant role in enhancing the electrocatalytic activity of the PtNi catalyst in the oxidation of methanol. The higher activity of GNS-supported metal with respect to carbon black- and carbon nanotube-supported metals was ascribed essentially to two factors, that is, the lower metal particle size of Me/GNS catalysts than that of the catalysts supported on other carbon structures, and the presence of oxygenated group on graphene surface. The lower metal particle size, due to the large surface area of graphene, gives rise to a large

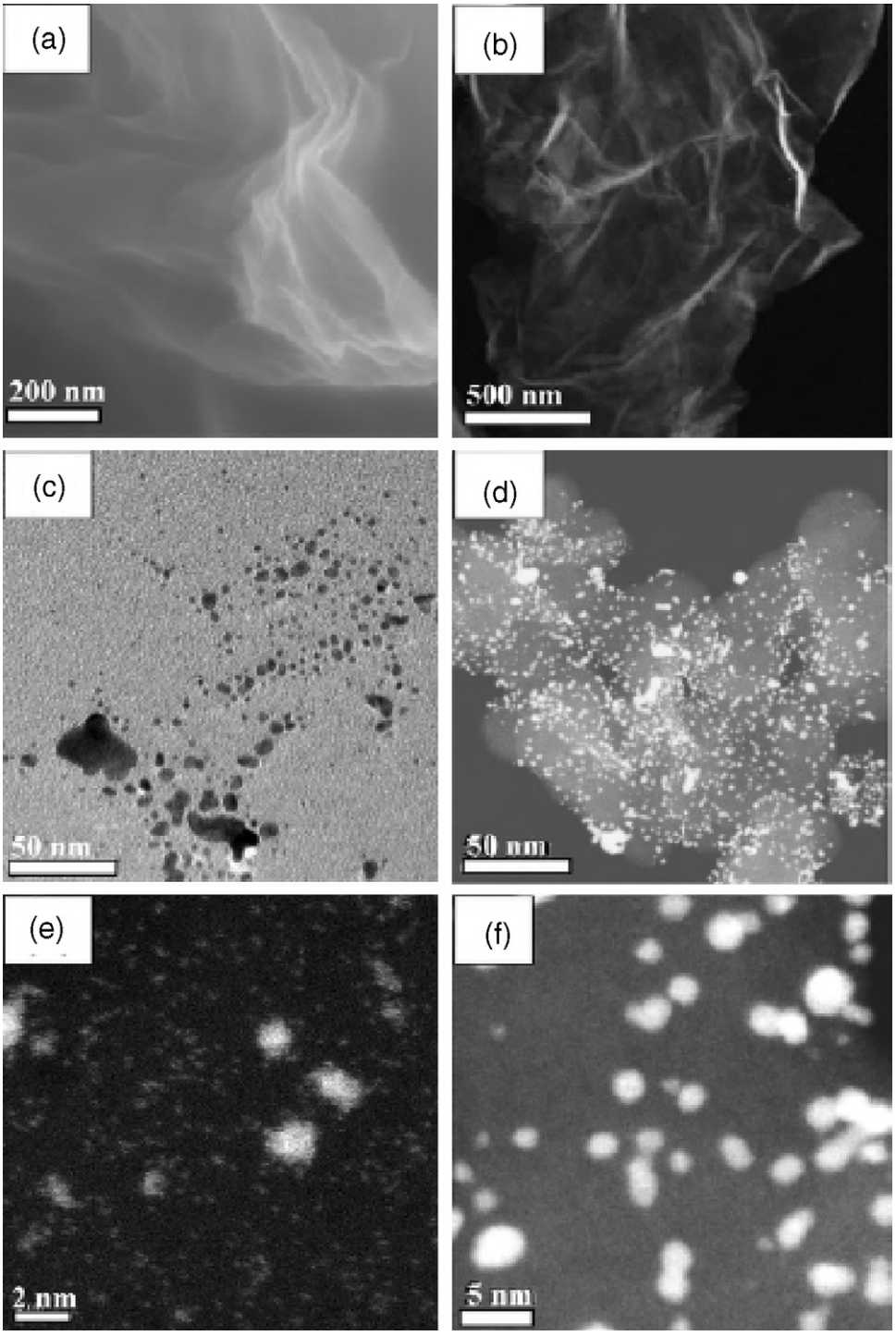

Fig. 9. SEM (a) and TEM (b) images of GNS. HAADF-STEM images of 20 wt% Pt/GNS (c) and 20 wt% Pt/CB (d). The magnification HAADF-STEM images of 20 wt% Pt/GNS (e) and 20 wt% Pt/CB (f).

Reproduced from Ref. [58], copyright 2011, with permission from Elsevier.

electrochemically active surface area of the catalyst. On the other hand, the oxygen-containing functional groups of GNS improve the electrocatalytic activity of Me/GNS catalysts by removing accumulated carbonaceous species that are formed during the oxidation of methanol. Xin et al. [47] submitted Pt/GNS, prepared by simultaneous reduction of GO and H_2PtCl_6 with $NaBH_4$, to heat treatment at 300 °C, and observed that heat treated Pt/GNS possess higher MOR activity and stability than untreated Pt/GNS. They ascribed the enhancement of the activity and stability to four effects induced by heat treatment: (1) enhancement of interaction between Pt and graphene; (2) additional Pt active sites exposed by the rolling of graphene sheets; (3) partial decomposition of surface functional groups, resulting in less defects on graphene; (4) change of Pt surface morphology from amorphous to more ordered states, giving rise to more active catalytic sites.

The catalytic activity of Me/GNS for the oxidation of other fuel such as hydrogen [58,80], hydrogen/carbon monoxide, ethanol [41,85] and formic acid [71,86,87] has also been investigated. CO

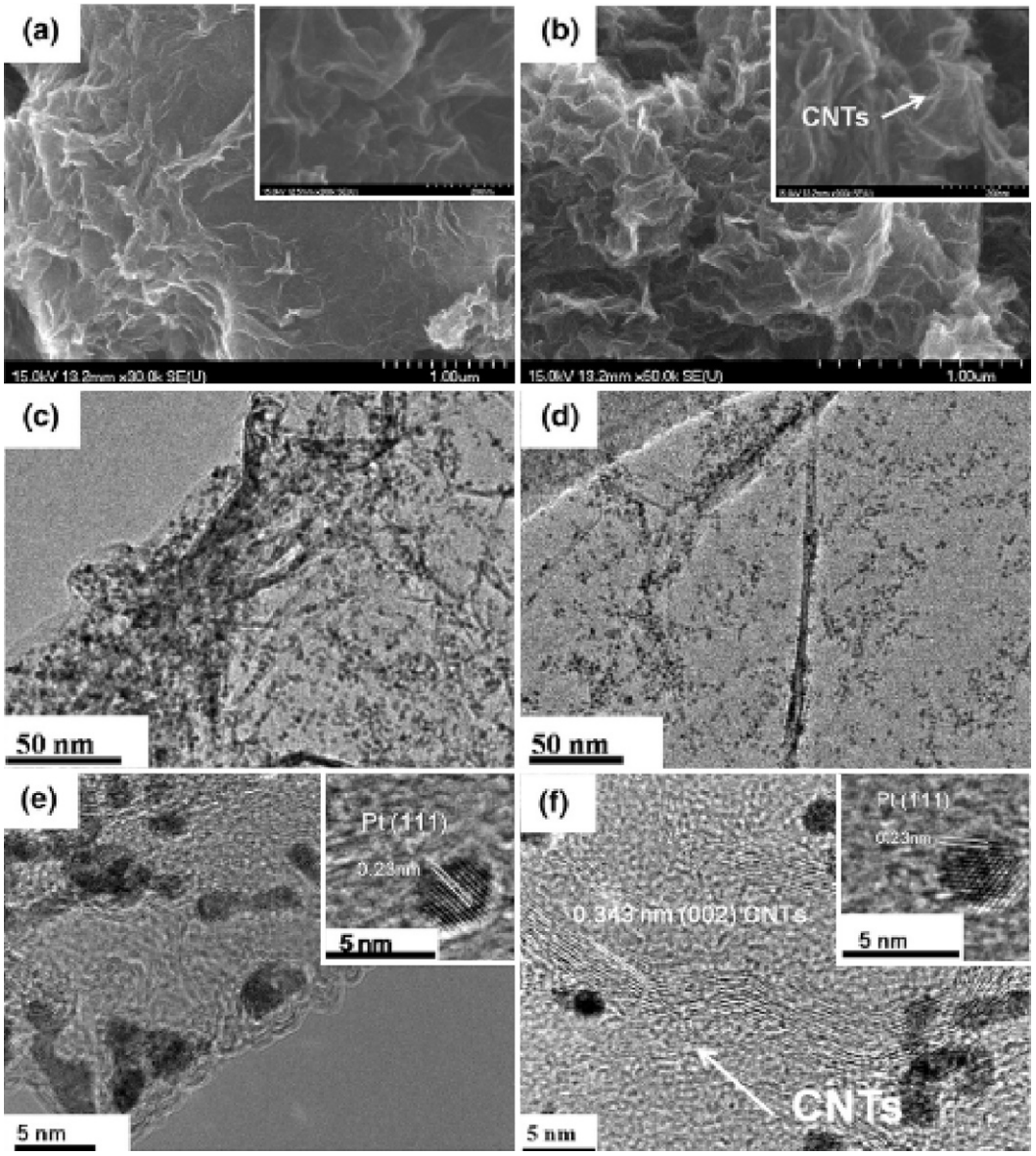

Fig. 10. (a, b) SEM, (c, d) the bright-field and (e, f) HR-lattice TEM images of (a, c, e) Pt/GNS and (b, d, f) Pt/GNS–CNTs; insets show the high magnification images. Reproduced from Ref. [77], copyright 2010, with permission from Elsevier.

poisoning is a major issue when reformate gas is used as a fuel in PEMFCs [88]. Yoo et al. [58,80] found that the Pt/GNS catalyst has a significantly higher CO tolerance than that of Pt/C. In pure H_2, the catalytic activities of Pt/GNS was slightly lower than those of Pt/C and PtRu/C. However, a more significant support effect was observed in the presence of H_2 with 500 ppm CO. The HOR activity of Pt/GNS was ca. 52% of that in pure H_2. In contrast, the Pt/C electrocatalyst was less than about 11% of the catalytic activity in H_2. In comparison, the PtRu/C, which is a well-known CO tolerant catalyst, maintained a catalytic activity of up to 45% under 500 ppm CO/H_2. This clearly shows that the CO tolerance performance of the Pt/GNS is significantly superior to that of Pt/C and that the substrate carbon material alters the catalytic properties of Pt. Two possible reasons for the excellent CO tolerant HOR activity of the Pt/GNS have been suggested. First, the presence of sub-nano-Pt clusters on the GNS may promote CO tolerance. Second, the chemical effect due to the modification of the Pt electronic structure by the GNS support may cause a difference in the catalytic activities.

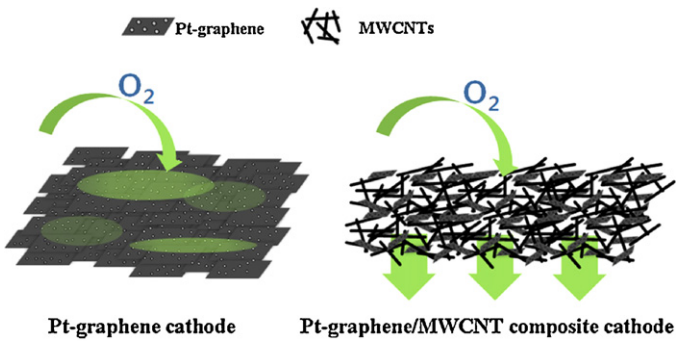

Fig. 11. The structures of the Pt–graphene cathode and Pt–graphene/MWCNT composite cathode.
Reproduced from Ref. [78], copyright 2011, with permission from Elsevier.

Compared with carbon black and graphite, graphene enhances considerably the electrocatalytic activity of Pt nanoparticles for ethanol oxidation by increasing the forward oxidation peak current density I_F and decreasing the reverse peak current density I_R (Table 3). Both I_F to I_R ratios for carbon black and graphite were less

Table 3
Comparison of electrocatalytic activity of ethanol oxidation on graphene-, carbon black-, and graphite-supported Pt nanoparticles.

Catalyst	Forward sweep		Reverse sweep		I_F/I_R ratio
	I_F (mA cm^{-2})	E (V)	I_R (mA cm^{-2})	E (V)	
Pt/GNS	16.2	0.72	4.4	0.48	3.66
Pt/C	13.8	0.65	15.3	0.46	0.90
Pt/Graphite	7.4	0.63	9.0	0.46	0.83

Reproduced from Ref. [41], copyright 2010, with permission from Elsevier.

than 1.0. As discussed above, the ratio describes the catalyst tolerance to CO-like intermediates formed on electrodes during the forward potential sweep. The high forward peak current density and the high I_F to I_R ratio for graphene-supported Pt nanoparticles indicate that graphene effectively enhances the complete oxidation of ethanol to CO_2, and fewer CO-like carbonaceous species accumulate on the electrode surface. Singh and Awasthi [85] observed that Pd nanoparticles dispersed on GNS have a higher electrocatalytic activity for ethanol oxidation in alkaline medium than those dispersed on nanocarbon particles or MWCNTs.

Finally, the activity for formic acid oxidation of GNS-supported Pd and Pt catalysts was higher than that of Pd/C and Pt/C, respectively [71,86,87].

4.1.1.2. Electro-catalytic activity of Me/GNS for oxygen reduction. A lesser amount of papers have been addressed to the activity for the oxygen reduction reaction (ORR) of Me/GNS than those dealing on the activity for methanol oxidation [43,45,47,59,81,89–91]. Conversely to the methanol oxidation, the comparison of the ORR activity of Me/GNS catalysts with that of carbon black supported catalysts indicated conflicting results. According to Ha et al. [45] and Li et al. [89], graphene-supported Pt showed a slightly higher ORR activity than the conventional carbon-supported Pt. Wu et al. [59] observed that Pt supported on carbon black has a similar initial half wave potential to that of Pt supported on graphene. Conversely, Xin et al. [47] observed a smaller ORR limiting current for Pt/GNS than that for Pt/C (Fig. 13). It was believed that the diffusion-limiting currents were strongly affected by the structure of the catalyst support. The sheet structure of graphene might slightly block oxygen diffusion compared with spherical carbon black particles. To support the results of Xin et al. [47], the performance of Pt/GNS as cathode catalyst in PEMFCs, as reported later, was lower than that of Pt/C

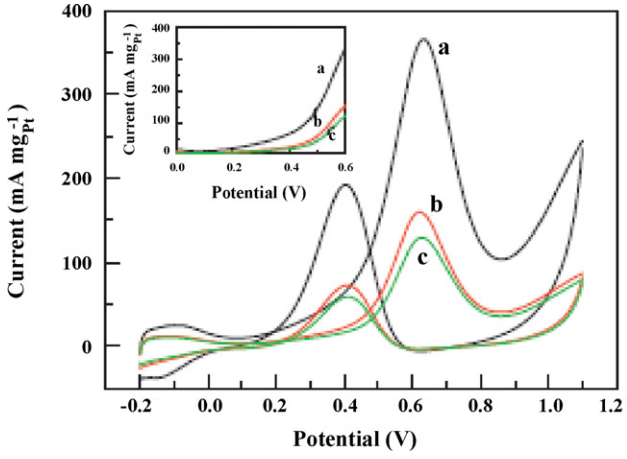

Fig. 12. The voltammetric responses of the oxidation of 0.5 M methanol in a 0.5 M H_2SO_4 aqueous solution at the PtNi catalyst with a Pt/Ni molar ratio of 1:1 supported on graphene (a), SWNTs (b), and Vulcan carbon (c). The scan rate was 50 mV s^{-1}. The inset shows the starting potential for methanol oxidation at the PtNi catalysts.
Reproduced from Ref. [48], copyright 2012, with permission from Elsevier.

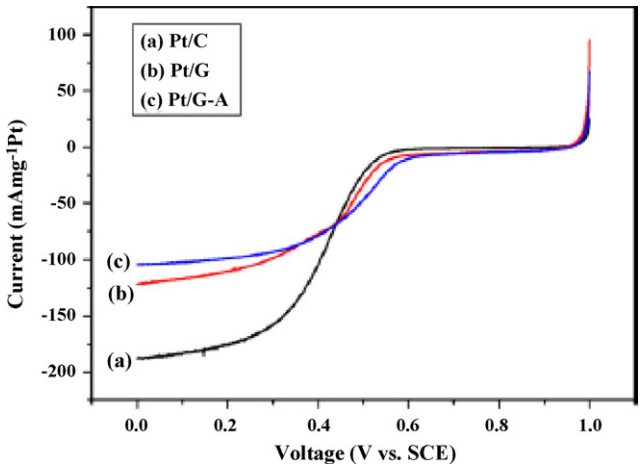

Fig. 13. Polarization curves for ORR on (a) Pt/C, (b) Pt/GNS (Pt/G) and (c) annealed Pt/GNs (Pt/G-A). O_2-saturated 0.5 M H_2SO_4 solution, scan rate: 5 mV s^{-1}, rotation rate: 2500 rpm.
Reproduced from Ref. [47], copyright 2011, with permission from Elsevier.

[64,78]. Finally, Sato et al. [90] found that, despite the similarity in Pt nanoparticle size, the oxygen reduction reaction was strongly affected by the size of graphene. Smaller sized graphene afforded higher mass and specific activity towards the oxygen reduction reaction.

4.1.2. Me supported on modified GNS

Different modified-GNS have been investigated as support for fuel cell catalysts, such as functionalized graphene by thermal exfoliation (f-GNS), poly(diallyldimethylammonium chloride) functionalized graphene (PDDA–GNS), nitrogen-doped–graphene (N–GNS), heteropolyacid molybdenum modified–graphene (PMo_{12}–GNS) and ethylenediamine-modified grapheme (ED- and EDTA–GNS).

The large amount of surface groups present on the surface of f-GNS may function as anchoring sites for Pt precursor to prevent the aggregation of the Pt nanoparticles, contributing to the good dispersion of Pt nanoparticles on GNS. Indeed, f-GNS allows to obtain supported metal having very low particle size at high metal loading on the support. As a consequence, the high active surface area of the catalysts results in an improved electrocatalytic activity for oxygen reduction [60,61] and, in particular, for methanol [37] and glycerol oxidation [62]. The oxidation of alcohol is enhanced also by the presence of oxygenated group on graphene surface, which remove accumulated carbonaceous species formed during alcohol oxidation.

Polyelectrolyte functionalization of GNS using PDDA stabilize metal nanoparticles on graphene support, resulting in a high dispersion of metal nanoparticles, especially at high metal loadings. Moreover, PDDA also stabilizes GNS against restacking during the electrochemical reactions. The advantages of PDDA functionalization on the electrocatalytic activity of GNSs is reported in various papers [44,65,66,92–95]. For example, Luo et al. [92] compared the MOR activity of 80 wt% Pt supported on GNS, PDDA–GNS and PDDA–C. Pt nanoparticles supported on PDDA–GNS showed higher electro-catalytic activity for methanol oxidation compared with Pt supported on both GNS and PDDA–C.

Nitrogen-doped carbon nanostructures and their composites demonstrate promising potential for fuel cell application [96]. Generally, Pt-based catalysts supported on nitrogen-doped carbons shows enhanced catalytic activity and durability toward oxygen reduction and methanol oxidation, which can be attributed to the high dispersion of Pt nanoparticles and the modified interaction

between Pt nanoparticles and the support [96]. Thus, nitrogen-doped graphene has been investigated as support for fuel cell catalysts. It has been shown using DFT that N-doping of graphene increases the binding energy of a Pt atom to the substrate [97]. In general, the more N atoms and the closer they are to the C atom which bonds directly to the Pt, the stronger the binding energy. This can be attributed to how N atoms want to form pentagonal structures. This disrupts the delocalized double bond typical of graphene sheets and causes the C–Pt bond to focus on their 2s/6s orbitals, respectively instead of their 2p/5d orbitals. This demonstrates the usefulness of using N-doped carbon structures as Pt catalyst supports since a two-fold increase in the binding energy was observed, resulting in an improvement of Pt catalyst durability and activity for oxygen reduction [98]. It was also shown that the molecular adsorption on Pt can be controlled by bonding disorders and vacancies in graphene lattice induced by nitrogen doping [99]. Heat treatment of graphene oxide with ammonia flow at various temperatures resulted in different distribution of nitrogen species [100]. Synchrotron based X-ray absorption near-edge structure (XANES) spectroscopy provides unambiguous evidence for the presence of three nitrogen species. The Pt/N–GNS, with N–GNS obtained by thermal treatment of GO at 800 °C, showed high electrocatalytic activity for methanol oxidation [100]. Xin et al. [101] prepared nitrogen doped graphene by via microwave heating in NH_3 atmosphere. The electrocatalytic activities toward methanol oxidation of Pt/GNS and Pt/N–GNS were compared by CV in CH_3OH/H_2SO_4. The peak current density in the forward sweep for Pt/N–GNS was almost 2 times of that of Pt/GNS.

A similar method to nitrogen-functionalization to improve the characteristics of GNS as supports for electrochemical reactions is the amino-functionalization. Murugesan et al. [87] observed a significant shift in the HCOOH oxidation onset potential on ethylenediamine functionalized graphene (ED–GNS) compared to GNS and carbon black supports. Wietecha et al. [102] reported the graphene functionalized with chelating groups and its application as fuel cell catalyst support. N-(trimethoxy-silylpropyl) ethylenediamine triacetic acid (EDTA–silane) can react with GO to form chelating groups modified graphene oxide (EDTA–GO) and then to form reduced chelating groups modified graphene oxide (EDTA–NGS). Compared to Pt/C, Pt/EDTA–GNS showed higher activity for methanol oxidation, longer stability, and excellent tolerance to CO poisoning.

Finally, it was shown that the addition of PMo_{12} benefits the dispersion of graphene nanosheets in water and the uniform dispersion of the PtRu nanoparticles on GNS: the PtRu/PMo_{12}–GNS catalysts have higher electrocatalytic activity and better electrochemical stability for methanol oxidation compared to PtRu/GNS [103].

4.1.3. *Me supported on hybrid GNS-PPy, GNS–SnO_2 and GNS–CNT supports*

Hybrid materials, such as polymer-carbon, ceramic-carbon and 1D carbon-2D carbon materials, possessing the properties of each component, or even with a synergistic effect, present improved characteristics with respect to the bare components. Thus, in the last years composite materials have been proposed as fuel cell catalyst supports [104]. These composite materials can possess more suitable properties for their use as catalyst supports than their individual components.

During the membrane electrode assembly (MEA) fabrication the surface area of GNS can decrease noticeably, due to the aggregation of the separated graphene sheets through the force of van der Waals and the interaction of π–π, although the separated graphene sheets exhibit large surface area, and this will decrease the performance of the catalysts supported on them. It is expected that the catalyst performance will be improved when 3D hybrid carbon materials

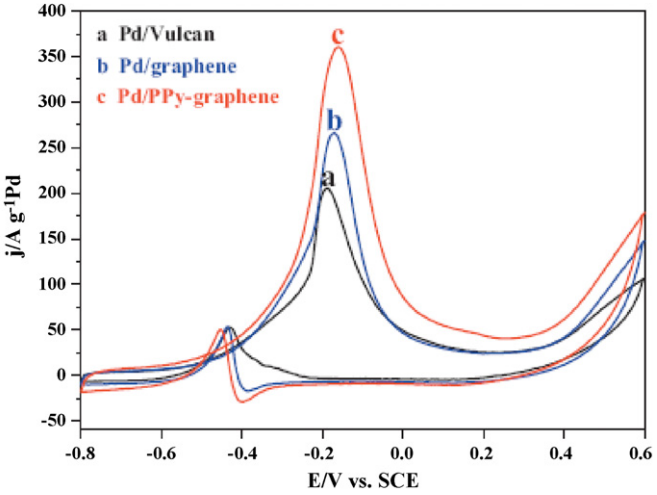

Fig. 14. CVs of Pd/Vulcan, Pd/graphene and Pd/PPy–graphene in 0.5 M NaOH + 1 M methanol at 25 °C and the scan rate of 50 mV s^{-1}.
Reproduced from Ref. [72], copyright 2011, with permission from Elsevier.

prepared from 1D (CNT or CF) and 2D (GNS) carbon materials are used as a support, considering that the graphene sheets will be separated by the 1D materials. This assumption has been attested by different works [76–78,105]. Chang et al. [105] found that Pt catalyst loaded on hybrid GNS-CF exhibits high electro-catalytic activity and good tolerance towards reaction intermediates than Pt/C and Pt/CF. Yang et al. [77] found that the electrochemically active surface area (ECSA) and the double-layer capacitance (C_{dl}) of Pt/GNS–CNTs are much higher than that of Pt/GNS and Pt/CNTs, revealing the synergistic effects between GNS and CNTs, which enhances the electrochemical activity of Pt nanoparticles and the electrolyte-accessible surface area. Yun et al. [78] investigated the electro-chemical activity of Pt/GNS–MWCNT composite cathodes. Electrochemical impedance spectroscopy measurements showed that the semicircular diameter of the Pt/GNS–MWCNT composite cathode plot was much smaller than that of the Pt/GNS cathode plot, suggesting that the ORR charge transfer resistance was much smaller at the Pt/GNS–MWCNT composite cathode catalysts that at Pt/GNS. Finally, Jha et al. [76] by CV measurements found that the MOR activity of PtRu/GNS–CNT is higher than that of both PtRu/GNS and PtRu/CNT.

The higher catalyst dispersion, together with the enhanced properties of the hybrid support, results in a high performance of the carbon-polymer supported catalysts [104]. Composite graphene–polypyrrole materials have been investigated as fuel cell catalyst supports [72–74]. The high catalyst dispersion of these hybrid materials was ascribed to the change from hydrophobic surface of pristine GNS to a more hydrophilic PPy coated-GNS surface. Moreover, the PPy may serve as "conducting bridges" among the graphene sheets. GNS–PPy supported catalysts showed high activity for methanol and formic acid oxidation [72,74]. Zhao et al. [72] investigated the activity for methanol electro-oxidation of Pd/GNS–PPy in an alkaline medium. The CVs of methanol oxidation on Pd/C, Pd/GNS and Pd/GNS–PPy are displayed in Fig. 14. The forward peak current density of Pd/GNS–PPy was higher than that of Pd/GNS and Pd/C, indicating that Pd/GNS–PPy composite has the highest activity for methanol oxidation. In the same way, the Pd/GNS–PPy catalysts showed high catalytic activity for formic acid electro-oxidation, particularly when the weight feed ratio of GO to pyrrole monomer is 2:1 [74].

The increase in the catalytic activity of catalysts supported on the hybrid ceramic–carbon composite was commonly ascribed to the synergic effect of the high electron conductivity of the

carbon, particularly of carbon nanotubes and graphene, with the co-catalytic properties of the ceramic material [104]. Moreover, carbon–ceramic materials presented higher corrosion resistance (by the presence of the oxide) than the single carbon materials. SnO_2 has been proposed as a support material for fuel cell electrocatalysts because of its chemical properties: it adsorbs OH species at low potentials and/or induces the electronic effect with Pt catalysts [106]. These properties promote the electro-oxidation on Pt of CO and low-molecular-weight alcohol, such as methanol and ethanol [107,108]. For its use as a catalyst support in fuel cells, however, the electrical conductance of SnO_2 has to be improved, by using metal-doped SnO_2 [109,110] or by mixing SnO_2 with a highly conductive carbon material, such as carbon nanotubes [111–113] or graphene [75]. Wen et al. [75] investigated the electro-catalytic activity for ethanol oxidation of Pd supported on hybrid GNS–SnO_2 materials with various GNS:SnO_2 ratios. The activity of Pd/GNS–SnO_2 was always higher than that of Pd/GNS, independently of SnO_2 content.

4.2. Long-term durability and short-term stability of Me/GNS

Long-term structural durability is one of the characteristics most necessary for fuel cells to be accepted as a viable product. The lifetime depends on fuel cell component materials, particularly the catalyst support [8,114]. Thus, in addition to the electrocatalytic activity, the durability of GNS-supported catalysts has also been evaluated. The electrochemically active surface area loss and electro-catalytic activity decrease of GNS-supported Pt have been evaluated by various durability tests, such as repetitive potential cycling (RPC) [44,58,60,101], potential holding method [59] and potential step method [65]) and compared with those of Pt/C [44,58–60,65] and Pt/CNT [65]. It was found that the ECSA loss and, as a consequence, the decrease of electro-catalytic activity for oxygen reduction [59,60] and hydrogen oxidation [58] of Pt/GNS following durability tests were lower than those of Pt/C. The loss of the ECSA and the electro-catalytic activity is directly related to Pt aggregation. Graphene sheets, with the presence of π sites and functional groups, may lead to a strong metal-support interaction and resultant resistance of Pt to sintering, and therefore enhanced durability. Also, strong interactions may occur between sub-nano-Pt clusters and GNS surface [58]. For example, the durability of both Pt/f-GNS and a commercial Pt/C catalysts was investigated by RPC for 5000 cycles in N_2-saturated 0.5 M H_2SO_4 [60]. The CV curve of Pt/f-GNS before RPC shows standard hydrogen adsorption/desorption peaks between 0.04 and 0.3 V, which are suppressed after 5000 cycles, indicating a decrease of the ECSA (Fig. 15a). Fig. 15b shows the ORR curves of Pt/f-GNS before and after RPC. It can be observed that the ORR curve shifts toward more negative potentials after 5000 cycles, meaning that the ORR activity of Pt/f-GNS ORR slightly decreased. Although some loss of the ECSA and ORR on Pt/f-GNS is observed, Pt/f-GNS shows higher initial value and good retention on both the ECSA and ORR activity compared with the commercial Pt/C catalyst (Fig. 15c). Both the initial ECSA and ORR activity of Pt/f-GNS are higher than that of Pt/C. The higher initial ECSA of Pt/f-GNS (108 $m^2\,g^{-1}$) than that of Pt/C (75 $m^2\,g^{-1}$) is ascribed to the smaller Pt particle size on the f-GNS than on C. Based on the average particle diameter of

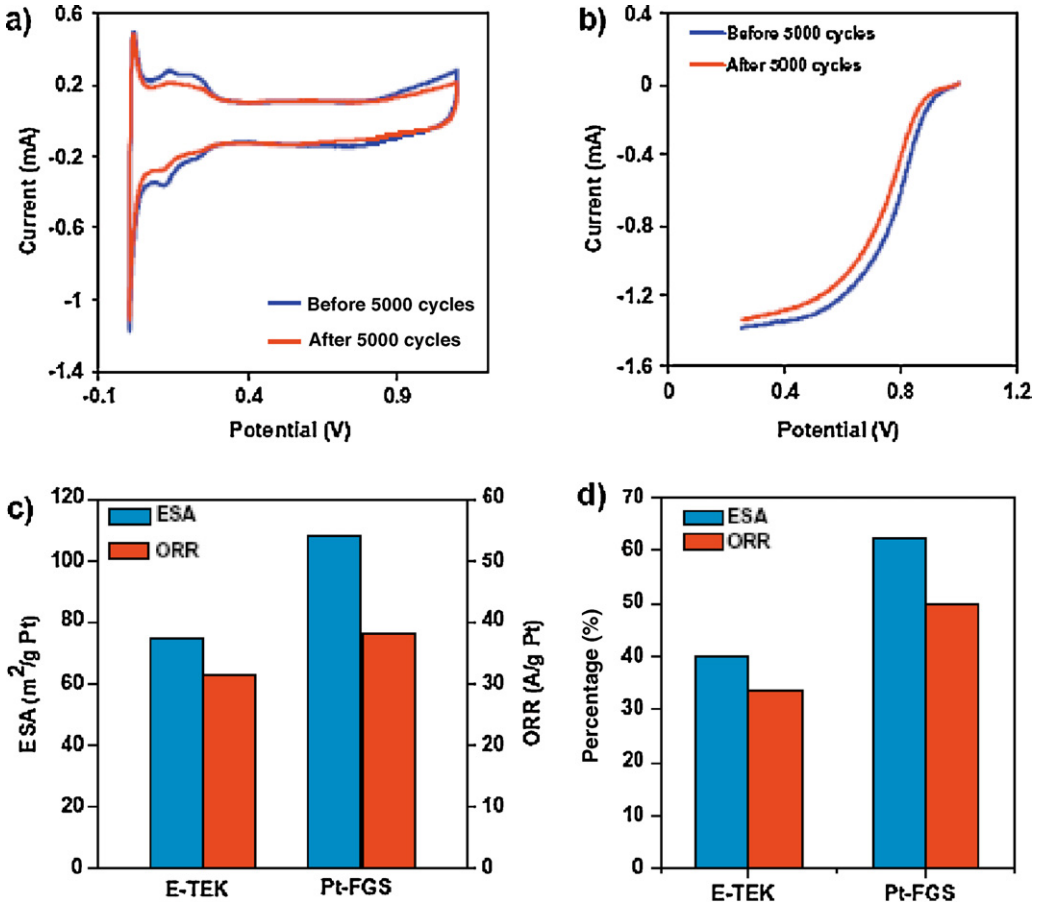

Fig. 15. Electrochemical properties tested in 0.5 M H_2SO_4 aqueous solution. (a) Cyclic voltammograms of Pt/f-GNS under a scan rate of 50 mV s^{-1} before and after 5000 CV degradation; (b) polarization curves for the O_2 reduction (10 mV s^{-1}, 1600 rpm) on Pt/f-GNS catalyst before and after 5000 cycles; (c) original values of ECSA and ORR activity at 0.9 V; (d) the percentage of retaining ECSA and ORR activity after 5000 CV degradation.

Reproduced from Ref. [60], copyright 2009, with permission from Elsevier.

2 nm for Pt on f-GNS, and 2.8 nm for Pt on Pt/C, the difference of the ECSA values is directly related to the difference in the particle size in inverse proportion. After RPC, this difference in the ECSA and ORR activity is further enhanced. The retained ECSA and ORR after 5000 cycles for Pt/f-GNS and Pt/C, compared with initial values, are shown in Fig. 15d. The ECSA of Pt/f-GNS after RPC retained 62.4% of the initial ECSA value. In comparison, commercial Pt/C catalyst retained only 40% of the initial ECSA. Similarly in ORR activity, Pt/f-GNS retained 49.8% of the original value while the commercial catalyst only 33.6%. Therefore, Pt/f-GNS is much more stable than the commercial Pt/C catalyst under this test condition.

Graphene nanoplatelets (GNPs) consist of layers (>10) of graphene sheets which might exhibit the advantageous properties of both single-layer graphene (high surface area, excellent conductivity [17] and mechanical strength) and highly ordered graphitic carbon (high stability, abundance in source and low cost). Shao et al. [65] employed GNP as an alternative support material for Pt nanoparticles. Pt nanoparticles were deposited on PDDA-coated GNP and CNT. The ORR activity of Pt/GNP toward oxygen reduction was comparable to Pt/CNT and a commercial Pt/C. However, the durability of Pt/GNP was greatly enhanced (2–3 times that of Pt/CNT and Pt/C). The high durability of Pt/GNP was attributed to the intrinsic high graphitization degree of GNP and the enhanced Pt–carbon interaction in Pt/GNP.

He et al. [44] investigated the effect of PDDA modification of graphene on the stability of GNS-supported Pt by RPC. After 3000 cycles, the Pt/GNS (without PDDA) showed a severe degradation (49.2%) as compared with that of Pt/PDDA–GNS (22.1%), due to Pt agglomeration and dissolution. After RPC, the ORR mass activity (MA), at a given potential of 0.85 V, decreases by 17.9% for the Pt/GNS (without PDDA) catalyst. For the Pt/PDDA–GNS catalyst, instead, the MA decreased by only 2.8%. PDDA not only acts as a binder or protecting agent for obtaining small and homogenous Pt nanoparticles on graphene sheets, but also stabilizes GNS against restacking during the reaction. Some supporting characteristic that might explain the origin of the enhanced durability of the PDDA associated catalysts are: (1) according to the XPS results, the electron transfer from Pt to N in PDDA decreases the oxidation degree of Pt, enhancing the durability of Pt nanoparticles [38]; and (2), Pt nanoparticles are more efficiently anchored onto GNS with the aid of PDDA, which prevents Pt from migrating/agglomerating on GNS and detaching from the support. Xin et al. [101] tested the durability of Pt/N–GNS and Pt/GNS by RPC. After 1000 cycles, the normalized ECSA of Pt/N–GNS retained 34.2% of the initial value, while that of Pt/GNS retained only 8.8% of the original ECSA.

In addition to the long-term structural stability of the catalysts, short-term stability, that is, the resistance to poisoning is an important parameter to evaluate the effectiveness of supported catalysts. Chronoamperometric (CA) experiments are widely applied to explore the catalytic stability of fuel cell catalysts. The short-term stability of the graphene supported catalysts has been assessed by CA tests (i–t curve) at constant potential [42,48,62,67,115–117]. Generally, CA profiles of methanol electro-oxidation show that the polarization currents decreased with time because the formation of intermediate species during methanol oxidation, inhibiting the reaction. From CA measurements, Kim et al. [62] observed that the current density for glycerol oxidation is in the order of PtRu/GNS > Pt/GNS > PtRu/C > Pt/C. The short-term stabilities of the PtNi/GNS, PtNi/SWCNT, and PtNi/C catalysts were evaluated by CA measurements under a constant potential of 0.64 V [48]. As can be seen in Fig. 16, the polarization currents at these catalysts decreased rapidly at the initial stage. However, after a time of 1000 s, the oxidation current at the PtNi/GNS catalyst (curve a) was still higher than the current at PtNi/SWCNT (curve b) and PtNi/C catalysts (curve c). This finding indicates that graphene can also enhance the electrocatalytic stability of the PtNi catalyst during methanol oxidation in comparison with SWCNT and carbon blacks.

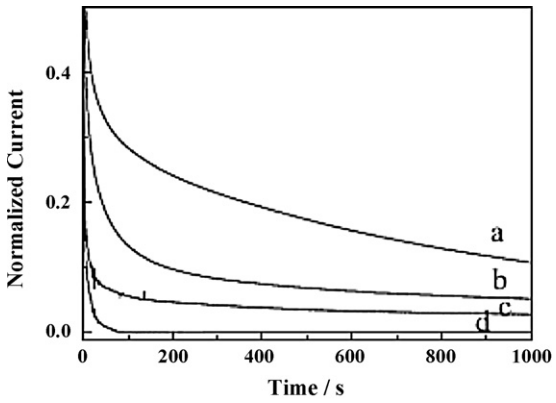

Fig. 16. Comparison of the stability of the PtNi catalyst with a Pt/Ni molar ratio of 1:1 supported on graphene (a), SWCNTs (b), and XC-72 carbon (c) for the electrochemical oxidation 0.5 M methanol in a 0.5 M H_2SO_4 aqueous solution under a constant potential of 0.64 V (vs. SCE). The currents presented in curves (a)–(c) were normalized with the highest current obtained at the PtNi/GNS, PtNi/SWCNT, and PtNi/C catalysts, respectively. Curve (d) is the amperometric response of PtNi/GNS catalyst in a 0.5 M H_2SO_4 aqueous solution without presence of methanol.
Reproduced from Ref. [48], copyright 2012, with permission from Elsevier.

4.3. Tests in fuel cells

From the practical point of view, the single cell test is the ultimate evaluation criterion for novel electrocatalysts materials. Compared to the number of paper on the catalytic activity of Me/GNS carried out by half-cell measurements, few works report tests of graphene supported catalysts in single fuel cells. Single PEMFC and DMFC tests using Pt and Pt_3Co catalysts supported on GNS as cathode materials have been carried out, indicating that GNS can be an effective support material [43,45,118,119]. Generally, no comparison of the activity of Pt/GNS with that of conventional Pt/C was made; when the activity of Pt/GNS was compared with that of Pt/C, the performance of Pt/GNS was similar [45] or even considerably lower [64,78] than that of Pt/C. During the MEA fabrication, as shown in Fig. 17a, graphene sheets tend to horizontally stack, owing to their 2D structure, resulting in a decrease of active sites at superimposed plane between graphene sheets. One strategy to increase Pt utilization is the addition of a spacing material to the catalyst layer. This may disrupt the preferred horizontal stacking of graphene sheets and make them randomly distributed in the catalyst layer, as can be seen in Fig. 17b. As a consequence, more Pt nanoparticles are effective for electrochemical fuel cell reactions in the presence of a spacer between graphene sheets. On this basis, Park et al. [64] tested in a single PEMFC a series of cathodes using Pt/GNS with different contents of carbon black in the catalyst layer. Carbon black was added as a spacer between graphene sheets in the catalyst layer. Fig. 18 shows the ECSA and C_{dl} of the cathodes with different carbon black content. The addition of carbon black in Pt/GNS catalyst layer increased the ECSA of for Pt nanoparticles. The ECSA is mainly controlled by (i) size of Pt nanoparticles dispersed on the support and (ii) Pt utilization. Since the distribution and size of Pt nanoparticles on the graphene sheets are not affected by addition of carbon black in the catalyst layer during the MEA fabrication, the increase of ECSA of the cathode has to be ascribed to a higher Pt utilization. Typically, the utilization of Pt dispersed on the catalyst support is proportional to the surface area of Pt nanoparticles in contact with electrolyte and it is intimately related to C_{dl}, which characterizes electrode-electrolyte interface. As can be seen in Fig. 18, the value of C_{dl} increases with the amount of carbon black in the catalyst layer. This result indicates that interface between

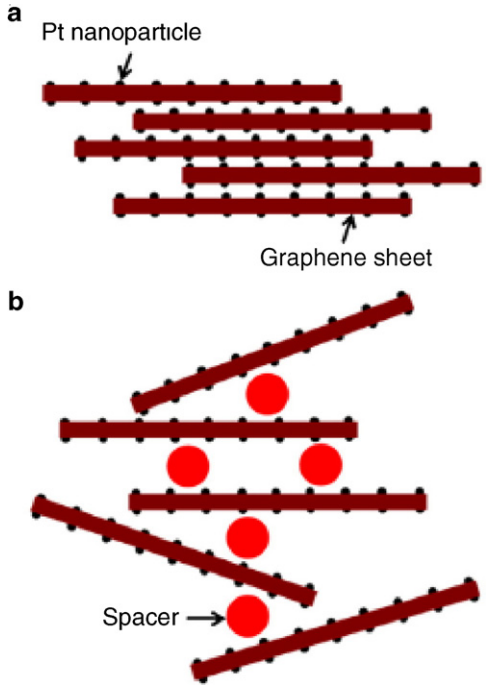

Fig. 17. Scheme showing the catalyst layer formed by (a) graphene sheets-supported Pt catalysts and (b) graphene sheets-supported Pt catalysts with a spacer. Reproduced from Ref. [64], copyright 2011, with permission from Elsevier.

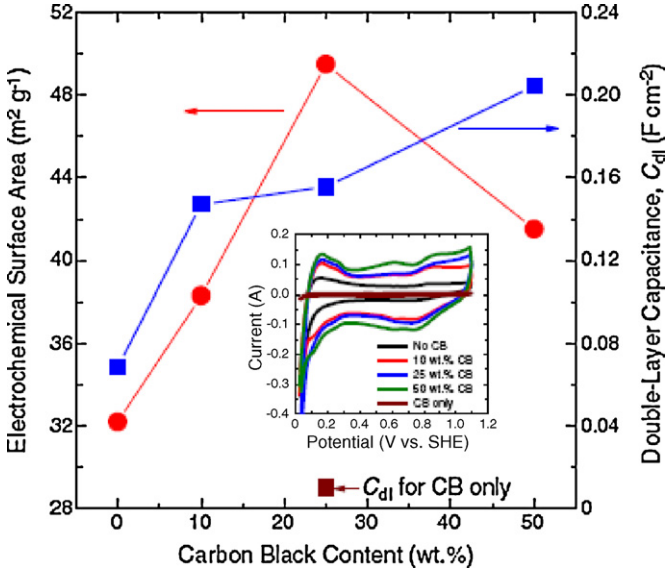

Fig. 18. Electrochemical surface area and double-layer capacitance of the cathodes prepared using graphene sheets-supported Pt catalyst with different carbon black content. The cathode was cycled at 50 mV s^{-1} between 0.02 and 1.1 V vs. SHE. Reproduced from Ref. [64], copyright 2011, with permission from Elsevier.

catalyst and ionomer increases with the carbon black added into the catalyst layer. Furthermore, it was clearly observed that the difference of C_{dl} between the cathodes with and without carbon black is significant. Apparently, carbon black increases Pt utilization by exposing a greater amount of Pt nanoparticles that would have been trapped between the superimposed graphene sheets in the absence of carbon black. On the other hand, the ECSA reaches a maximum with addition of 25 wt% carbon black, and then it decays with increasing carbon content, while the value of C_{dl} continues to increase with carbon loading in the catalyst layer. i.e., excess carbon black in the catalyst layer does not help increase utilization of Pt involved in ionic network, reflecting that there exists trade-off between extending and screening effective Pt surface area with addition of carbon black as a spacer in the catalyst layer. The performance of the single PEMFC using graphene sheets-supported Pt catalyst with carbon black as cathode material considerably increased with respect to that of a PEMFC using Pt/GNS without carbon black, and was comparable to that of a commercial Pt/C catalyst. Another strategy, as reported in Section 4.1.3, is the use of hybrid GNS–CNT supports. It is expected that the catalyst performance will be improved when 3D hybrid carbon materials prepared from 1D (CNT or CF) and 2D (GNS) carbon materials are used as a support, considering that the graphene sheets will be separated by the 1D materials when the 1D and the 2D GNS structures are combined. Tests in PEMFCs and DMFCs of catalysts supported on hybrid GNS–CNT as electrode materials have been carried out [76,78,120,121]. The performance of the cells with GNS–CNT supported catalysts was better than that of the cells with catalysts supported on bare GNS and bare CNT. Lv et al. [120] deposited PtRu nanoparticles with 2–4 nm size on a hybrid N-doped carbon nanotube–graphene hybrid support, in which the graphene layers are distributed inside the CNT inner cavities. Compared to the catalysts supported on CNTs and

Table 4
Characteristics and electrocatalytic activity of catalysts supported on bare GNS. Synthesis method: 1M, simultaneous metal precursors and GO reduction (one-step method); 2M, sequential GO and metal precursors reduction (two-step method). Test: hc, half cell; fc, fuel cell.

Support/synthesis method	Catalyst particle size/metal loading nm/wt%	Chemical reaction/test	Electrocatalytic activity: comparison with other carbon supports	References
GNS/1 M	Pt,PtRu n.d./n.d.	MOR, EOR/hc.	Pt/GNS > PtRu/Vulcan, PtRu/G	[41]
GNS/1 M	Pt 5–6/45	MOR/hc	Pt/GNS > Pt/Vulcan	[46]
GNS/1 M	Pt 5/10	MOR/hc	Pt/GNS > Pt/Vulcan	[47]
GNS/1 M	PtNi 35/n.d.	MOR/hc	PtNi/GNS > PtNi/Vulcan, PtNi/SWNT	[48]
GNS/1 M	Pt n.d/n.d.	MOR/hc	Pt/GNS > Pt/Vulcan	[55]
GNS/1 M	PtRu 2.5/80	MOR/hc	PtRu/GNS > PtRu/Vulcan	[56]
GNS/2 M	Pt 2.5/20	MOR/hc	Pt/GNS > Pt/CB	[80]
GNS/1 M	Pt n.d/n.d.	MOR/hc	Pt/GNS > Pt/Vulcan	[82]
GNS/1 M	Pt 2.75/n.d.	MOR/hc	Pt/GNS > Pt/MWCNT	[40]
GNS/2 M	PtRu 2.2/n.d.	MOR/hc	PtRu/GNS > PtRu/MWCNT	[79]
GNS/2 M	Pd 2.5/20	MOR,EOR/hc	Pd/GNS > Pd/MWCNT	[85]
GNS/2 M	Pt 2.5/20	HOR/hc	Pt/GNS < Pt/CB	[58]
GNS/2 M	Pd 3/n.d.	FAOR/hc	Pd/GNS > Pd/Vulcan	[71]
GNS/1 M	Pt 2.9/70	ORR/hc	Pt/GNS ≥ Pt/Vulcan	[45]
GNS/2 M	Pt 3.1/n.d.	ORR/hc	Pt/GNS > Pt/Vulcan	[89]
GNS/2 M	Pt n.d./n.d.	ORR/hc	Pt/GNS = Pt/Vulcan	[59]
GNS/1 M	Pt 5/10	ORR/hc	Pt/GNS < Pt/Vulcan	[47]
GNS/1 M	Pt 2.2/50	ORR/fc	Pt/GNS « Pt/Vulcan	[78]

Table 5
Characteristics and electrocatalytic activity of catalysts supported on modified GNS and on composite GNS-containing materials. Synthesis method: 1M, simultaneous metal precursors and GO reduction (one-step method); 2M, sequential GO and metal precursors reduction (two-step method). Test: hc, half cell; fc, fuel cell.

Support/synthesis method	Catalyst particle size/metal loading nm/wt%	Chemical reaction/Test	Electrocatalytic activity: comparison with other carbon supports	References
f-GNS/2M	Pt 1.8–2.9/40–80	MOR/hc	Pt/GNS >Pt/Vulcan	[37]
f-GNS/2M	Pt,PtRu 1.8–2.2/60	GlyOR/hc	PtRu/GNS >PtRu/Vulcan	[62]
f-GNS/2M	Pt 2–6/20	ORR/hc	Pt/GNS >Pt/Vulcan	[60]
f-GNS/2M	Pt 4/20	ORR/fc	Pt/GNS «Pt/Vulcan	[64]
PDDA–GNS/1M	Pt 2/40	ORR/hc	Pt/PDDA–GNS > Pt/GNS	[4]
PDDA–GNS/2M	Pt 3.5/n.d.	ORR/hc	Pt/PDDA–GNS ≈ Pt/Vulcan, Pt/CNT	[65]
PDDA–GNS/2M	Pt 2.6,4.5/40,80	MOR/hc	Pt/PDDA–GNS > Pt/GNS,Pt/PDDA–C	[94]
N–GNS/2M	Pt n.d./n.d.	ORR/fc	Pt/N–GNS > Pt/GNS	[119]
N–GNS/2M	Pt 2.5./n.d.	MOR/hc	Pt/N–GNS > Pt/GNS	[101]
ED-GNS/2M	Pt n.d./n.d.	FAOR/hc	Pt/ED-GNS > Pt/GNS,Pt/C	[87]
ED-GNS/1M	Pt 2.2–4.6/n.d.	MOR/hc	Pt/ED-GNS > Pt/GNS,Pt/C,Pt/CNT	[102]
f-GNS–CNT/2M	PtRu 5–10/40	MOR/hc	Pt/GNS–CNT > Pt/GNS > Pt/CNT	[76]
GNS–CNT/1M	Pt 2–2.4/20	HOR/hc	Pt/GNS-NT > Pt/GNS > Pt/CNT > Pt/C	[77]
GNS–CNT/1M	Pt 2.2/50	ORR/fc	Pt/CB > Pt/GNS-MWNT > Pt/GNS	[78]
f-GNS–CNT/2M	Pt,PtRu 7.5/n.d.	ORR,MOR/fc	Pt/50GNS-50MWNT > Pt/MWNT	[76]
GNS-N-CNT/2M	PtRu 2–4/n.d.	MOR/fc	PtRu/GNS–NCNT > PtRu/CNT > PtRu/C	[120]
GNS-CF/2M.	Pt 3–7/n.d.	MOR/hc	Pt/GNS–CF > Pt/CF > Pt/C	[105]
GNS–PPy/2M	Pt 6/25	MOR	Pt/GNS–CNNT > Pt/GNS > Pt/Vulcan	[72]
GNS–SnO_2/2M.	Pt 1.5/20	EOR	Pt/GNS–SnO_2 > Pt/GNS	[75]

conventional carbon black, a higher activity for methanol oxidation and an improved single-cell performance were achieved by a synergistic effect of the hierarchical structure (hybrid GNS–CNT) and electronic modulation (N-doping). Yun et al. [78] prepared GNS–MWCNT supported Pt catalysts and tested their suitability as cathode materials in PEMFCs. The performance of the Pt/GNS–MWCNT composite cathode was much higher than that of the Pt/GNS, but slightly lower than that of Pt/C. The maximum power density of the Pt/GNS–MWCNT composite cathode was four fold higher compared than that of the Pt/GNS cathode. The maximum power density of the Pt/GNS–MWCNT composite cathode (0.13 mg Pt/cm^2) was only 17% lower than that of the Pt–carbon black cathode with a 35% higher Pt loading (0.2 mg Pt/cm^2). Jha et al. [76] and Jafri et al. [121] prepared f-GNS–f-CNT supported Pt and PtRu catalysts by varying the f-GNS/f-CNT weight ratio, and used them as electrocatalysts in PEMFCs [121] and in DMFCs [76]. In both cases, the best performance was obtained using catalysts supported on GNS–CNT in the GNS/CNT weight ratio of 1 as cathode materials for oxygen reduction [76,121] as well as anode materials for methanol oxidation [76]. The performance of all GNS–CNT supported catalysts was higher than that of CNT supported catalysts.

5. Conclusions

The combination of the high surface area, high conductivity, unique graphitized basal plane structure and potential low manufacturing cost makes graphene sheets a promising candidate as catalyst support in low-temperature fuel cells. So, typical fuel cell catalysts supported on GNS have been synthesized and characterized, and their electrocatalytic activity for chemical reactions of interest for an eventual use in fuel cells has been investigated by half-cell measurements and tests in single fuel cells have also been performed.

The synthesis of Me/GNS by deposition of metal precursors on the hydrophilic GO, followed by simultaneous oxidation of GO and metal precursors is preferred to the synthesis by reduction of GO followed by deposition and reduction of metal precursor (sequential method), because it is hard to deposit metal nanoparticles on the hydrophobic graphene.

Generally, using graphene sheets as a support very low metal particle size is obtained, lower than the particle size obtained by using other carbon supports. Low particle size is obtained also for high metal loadings on GNS. The benefits of the use of GNS as catalyst support are further improved by its functionalization, giving rise to a higher and more homogeneous metal dispersion, which in turns increases the electrocatalytic activity. Moreover, the presence of oxygen- and/or nitrogen-containing group on GNS surface, particularly on functionalized GNS surface, assists the oxidation of poisoning species adsorbed on the catalyst, coming to the partial oxidation of alcohols. It was also reported that the formation of sub-nano-Pt clusters promoted by graphene may improve the CO tolerance. Thus, Me/GNS catalysts have a significantly higher tolerance to poisoning species than that of Me/C catalysts, and the presence of GNS enhances the complete oxidation of methanol to CO_2. Indeed, there is a general consensus regarding the effectiveness of the use of graphene-supported catalysts as anode materials in DMFCs. The catalytic activity for methanol oxidation of Me/GNS was always higher that that of Me/C and/or Me/CNT [37,40,41,46–48,55,56,79,80,82,85,87,92,102].

The catalytic activity for hydrogen oxidation of Me/GNS, instead, was about 40% lower than that of Pt/C with similar Pt particle size [58]. Thus, in the absence of poisoning species, the effect of GNS support on the catalytic activity is negative. A higher activity for the HOR, however, was observed in the presence of CO, in agreement with the results found for alcohol oxidation. This means that the positive effect of GNS as support for alcohol and CO oxidation is not due to the higher catalyst dispersion on graphene surface, but has to be ascribed to the co-catalytic effect of oxygen and/or nitrogen species, and also to the presence of sub-nano-metal clusters, on the GNS surface.

Controversial results regarding the activity for oxygen reduction of Me/GNS have been reported by half-cell measurements [45,47,59,60,65,89]. Higher [60,89], similar [45,59,65] and lower [47] ORR activity than Me/C has been observed. Moreover, fuel cell tests with Pt/GNS catalysts as cathode materials showed a considerably lower performance than that of the cell with Pt/C as cathode catalyst. It was believed that the ORR diffusion-limiting currents were strongly affected by the structure of the catalyst supporting material. The sheet structure of graphene might block oxygen diffusion a little bit compared with spherical carbon black particles [47]. Thus, the ordered flat structure of grapheme should be less effective than the spherical structure of carbon blacks, randomly distributed in the catalyst layer. The characteristics and electrocatalytic activity of catalysts supported on bare GNS, on functionalized GNS and on composite GNS-containing materials are shown in Tables 4 and 5.

Higher structural durability of GNS-supported catalysts submitted to fuel cell operation conditions than that of conventional carbon and carbon nanotube supported catalysts was observed

[44,58–60,65], essentially ascribed to strong metal–graphene interactions. Particularly, high durability of functionalized GNS has been reported. CA tests indicates that graphene can also enhance the short term electrocatalytic stability of the catalyst during methanol oxidation in comparison with carbon nanotubes and carbon blacks.

The use of hybrid GNS-containing materials, such as GNS–PPy, GNS–SnO_2 and GNS–CNT as fuel cell catalyst supports was very promising. Catalysts supported on these composite materials presented a higher catalytic activity than those supported on of single components.

Compared to the number of paper on the catalytic activity of Me/GNS carried out by half-cell measurements, few works report tests of graphene supported catalysts in single fuel cell. A problem regarding the use of Me/GNS in fuel cell has been reported [64]. During the MEA fabrication, graphene sheets as a support for catalysts tend to be horizontally stacked due to their two-dimensional structure, resulting in a loss of active sites at superimposed plane between graphene sheets. One strategy to increase Pt utilization is based on the addition of a spacing material such as carbon black particles to the catalyst layer [64]. This may disrupt the preferred horizontal stacking of graphene sheets and make them randomly distributed in the catalyst layer. Another strategy is to increase the space between graphene by the use of hybrid GNS–CNT supports. The graphene sheets will be separated by the 1D materials when the 1D and the 2D GNS structures are combined. Fuel cells with catalysts supported on composite GNS–CNT materials better performed than the cells with catalysts supported on single GNS and CNT [76,78,120,121].

Summarizing, GNS-supported catalysts possess higher activity for the oxidation of small organic molecules (SOM) than that of conventional carbon black supported catalysts. Regarding hydrogen oxidation and oxygen reduction, instead, GNS-supported catalysts have a similar or lower activity than that of Me/C. As the surface area of GNS supported catalysts is commonly higher than that of catalysts supported on other carbon support, their activity should be higher for all the chemical reactions. Being the activity of Me/GNS higher for SOM oxidation and similar/lower for oxygen reduction and hydrogen oxidation, it should mean that the direct effect of support on the activity is more important than the indirect effect on the active surface area of the catalyst. Indeed, the co-catalytic effect of oxygen- and/or nitrogen-containing species on graphene surface makes GNS excellent fuel cell catalyst supports in the presence of poisoning species deriving from partial alcohol oxidation or reformate fuel. In the absence of poisoning species, however, as in the case of the HOR and ORR, the suitability of GNS as fuel cell catalyst support is similar or lower than that of the other carbon supports. Thus, GNS-supported catalysts are suitable to substitute conventional carbon black supported catalysts as anode materials in direct alcohol fuel cells and in PEMFCs fuelled with reformate gas. It is not advantageous, however, the substitution of Pt/C with Pt/GNS as a cathode material in all low-temperature fuel cells.

References

[1] A.K. Geim, K.S. Novoselov, Nature Materials 6 (2007) 183–191.
[2] D. Chen, L. Tang, J. Li, Chemical Society Reviews 39 (2010) 3157–3180.
[3] D.A.C. Brownson, D.K. Kampouris, C.E. Banks, Journal of Power Sources 196 (2011) 4873–4885.
[4] K.S. Novoselov, A.K. Geim, S.V. Morozov, D. Jiang, Y. Zhang, S.V. Dubonos, I.V. Grigorieva, A.A. Firsov, Science 306 (2004) 666–669.
[5] K.S. Novoselov, A.K. Geim, S.V. Morozov, D. Jiang, M.I. Katsnelson, I.V. Grigorieva, S.V. Dubonos, A.A. Firsov, Nature 438 (2005) 197–200.
[6] V. Singh, D. Joung, L. Zhai, S. Das, S.I. Khondaker, S. Seal, Progress in Materials Science 56 (2011) 1178–1271.
[7] E. Antolini, Materials Chemistry and Physics 78 (2003) 563–573.
[8] E. Antolini, Applied Catalysis B 88 (2009) 1–24.
[9] S. Stankovic, D.A. Dikin, G.H.B. Dommett, K.M. Kohlhass, E.J. Zimney, E.A. Stach, R.D. Piner, S.T. Nguyen, R.S. Ruoff, Nature 442 (2006) 282–286.
[10] Y.X. Xu, H. Bai, G.W. Lu, C. Li, G.Q. Shi, Journal of the American Chemical Society 130 (2008) 5856–5857.
[11] J. Hou, Y. Shao, M.W. Ellis, R.B. Moore, B. Yi, Physical Chemistry Chemical Physics 13 (2011) 15384–15402.
[12] Y. Sun, Q. Wu, G. Shi, Energy and Environmental Science 4 (2011) 1113–1132.
[13] X. Huang, Z. Yin, S. Wu, X. Qi, Q. He, Q. Zhang, Q. Yan, F. Boey, H. Zhang, Small 7 (2011) 1876–1902.
[14] C. Berger, Z.M. Song, X.B. Li, X.S. Wu, N. Brown, C. Naud, D. Mayou, T. Li, J. Hass, A.N. Marchenkov, E.H. Conrad, P.N. First, W.A. de Heer, Science 312 (2006) 1191–1198.
[15] A. Dato, V. Radmilovic, Z. Lee, J. Phillips, M. Frenklach, Nano Letters 8 (2008) 2012–2016.
[16] M. Choucair, P. Thordarson, J.A. Stride, Nature Nanotechnology 4 (2009) 30–33.
[17] N. Liu, F. Luo, H. Wu, Y. Liu, C. Zhang, J. Chen, Advanced Functional Materials 18 (2008) 1518–1525.
[18] G. Wang, B. Wang, J. Park, Y. Wang, B. Sun, J. Yao, Carbon 47 (2009) 3242–3246.
[19] S.H. Lee, S.D. Seo, Y.H. Jin, H.W. Shim, D.W. Kim, Electrochemistry Communications 12 (2010) 1419–1422.
[20] M. Alanyalıoğlu, J.J. Segura, J. Oró-Solè, N. Casañ-Pastor, Carbon 50 (2012) 142–152.
[21] H. He, T. Riedl, A. Lerf, J. Klinowski, Journal of Physical Chemistry 100 (1996) 19954–19958.
[22] A. Lerf, H. He, T. Riedl, M. Forster, J. Klinowski, Solid State Ionics 101–103 (1997) 857–862.
[23] C. Hontoria-Lucas, A.J. Lopez-Peinado, J.d.D. Lopez-Gonzalez, M.L. Rojas-Cervantes, R.M. Martin-Aranda, Carbon 33 (1995) 1585–1592.
[24] B.C. Brodie, Annales de Chime et de Physique 59 (1860) 466–472.
[25] L. Staudenmaier, Chemische Berichte 31 (1898) 1481–1499.
[26] W.S. Hummers, R.E. Offeman, Journal of the American Chemical Society 80 (1958) 1339.
[27] G.I. Titelman, V. Gelman, S. Bron, R.L. Khalfin, Y. Cohen, H. Bianco-Peled, Carbon 43 (2005) 641–649.
[28] A.B. Bourlinos, D. Gournis, D. Petridis, T. Szabo, A. Szeri, I. Dekany, Langmuir 19 (2003) 6050–6055.
[29] U. Hofmann, A. Frenzel, Kolloid-Zeitschrift and Zeitschrift fur Polymere 68 (1934) 149–151.
[30] S. Stankovich, D.A. Dikin, R.D. Piner, K.A. Kohlhaas, A. Kleinhammes, Y. Jia, Y. Wu, S.T. Nguyen, R.S. Ruoff, Carbon 45 (2007) 1558–1565.
[31] B. Saner, F. Okyay, Y. Yürüm, Fuel 89 (2010) 1903–1910.
[32] G.K. Ramesha, S. Sampath, Journal of Physical Chemistry C 113 (2009) 7985–7989.
[33] Z. Wang, X. Zhou, J. Zhang, F. Boey, H. Zhang, Journal of Physical Chemistry C 113 (2009) 14071–14075.
[34] V.S. Dilimon, S. Sampath, Thin Solid Films 519 (2011) 2323–2327.
[35] H.C. Schniepp, J.-L. Li, M.J. McAllister, H. Sai, M. Herrera-Alonso, D.H. Adamson, R.K. Prud'homme, R. Car, D.A. Saville, I.A. Aksay, Journal of Physical Chemistry B 110 (2006) 8535–8539.
[36] M.J. McAllister, J.-L. Li, D.H. Adamson, H.C. Schniepp, A.A. Abdala, J. Liu, M. Herrera-Alonso, D.L. Milius, R. Car, R.K. Prud'homme, I.A. Aksay, Chemistry of Materials 19 (2007) 4396–4404.
[37] S.M. Choi, M.H. Seo, H.J. Kim, W.B. Kim, Carbon 49 (2011) 904–909.
[38] C. Xu, X. Wang, J.W. Zhu, Journal of Physical Chemistry C 112 (2008) 19841–19845.
[39] Y. Si, E.T. Samulski, Chemistry of Materials 20 (2008) 6792–6797.
[40] Y. Li, W. Gao, L. Ci, C. Wang, P.M. Ajayan, Carbon 48 (2010) 1124–1130.
[41] L. Dong, R.R.S. Gari, Z. Li, M.M. Craig, S. Hou, Carbon 48 (2010) 781–787.
[42] Y. Zhang, Y. Gu, S. Lin, J. Wei, Z. Wang, C. Wang, Y. Du, W. Ye, Electrochimica Acta 56 (2011) 8746–8751.
[43] C.V. Rao, A.L.M. Reddy, Y. Ishikawa, P.M. Ajayan, Carbon 49 (2011) 931–936.
[44] W. He, H. Jiang, Y. Zhou, S. Yang, X. Xue, Z. Zou, X. Zhang, D.L. Akins, H. Yang, Carbon 50 (2012) 265–274.
[45] H.-W. Ha, I.Y. Kim, S.-J. Hwang, R.S. Ruoff, Electrochemical and Solid-State Letters 14 (2011) B70–B73.
[46] Y. Li, L. Tang, J. Li, Electrochemistry Communications 11 (2009) 846–849.
[47] Y. Xin, J. Liu, Y. Zhou, W. Liu, J. Gao, Y. Xie, Y. Yin, Z. Zou, Journal of Power Sources 196 (2011) 1012–1018.
[48] Y. Hu, P. Wu, Y. Yin, H. Zhang, C. Cai, Applied Catalysis B 111/112 (2012) 208–217.
[49] Y. Qian, C. Wang, Z. Le, Applied Surface Science 257 (2011) 10758–10762.
[50] Y. Wang, J. Liu, L. Liu, D.D. Sun, Nanoscale Research Letters 6 (2011) 241–248.
[51] H. Zhang, X. Xu, P. Gu, C. Li, P. Wu, C. Cai, Electrochimica Acta 56 (2011) 7064–7070.
[52] C.-S. Liao, C.-T. Liao, C.-Y. Tso, H.-J. Shy, Materials Chemistry and Physics 130 (2011) 270–274.
[53] S. Liu, L. Wang, J. Tian, W. Lu, Y. Zhang, X. Wang, X. Sun, Journal of Nanoparticle Research 13 (2011) 4731–4737.
[54] P. Kundu, C. Nethravathi, P.A. Deshpande, M. Rajamathi, G. Madras, N. Ravishankar, Chemistry of Materials 23 (2011) 2772–2780.
[55] S. Sharma, A. Ganguly, P. Papakonstatinou, X. Miao, M. Li, J.L. Hutchison, M. Delichatsios, S. Ukleja, Journal of Physical Chemistry C 114 (2010) 10466–19459.
[56] S. Bong, Y.R. Kim, I. Kim, S. Woo, S. Uhm, J. Lee, H. Kim, Electrochemistry Communications 12 (2010) 129–131.
[57] Y. Hu, J. Jin, P. Wu, H. Zhang, C. Cai, Electrochimica Acta 56 (2010) 491–500.

[58] E. Yoo, T. Okada, T. Akita, M. Kohyama, I. Honma, J. Nakamura, Journal of Power Sources 196 (2011) 110–115.
[59] H. Wu, D. Wexler, H. Liu, Journal of Solid State Electrochemistry 15 (2011) 1057–1062.
[60] R. Kou, Y. Shao, D. Wang, M.H. Engelhard, J.H. Kwak, J. Wang, V.V. Viswanathan, C. Wang, Y. Lin, Y. Wang, I.A. Aksay, J. Liu, Electrochemistry Communications 11 (2009) 954–957.
[61] M.H. Seo, S.M. Choi, H.J. Kim, W.B. Kim, Electrochemistry Communications 13 (2011) 182–185.
[62] H.J. Kim, S.M. Choi, M.H. Seo, S. Green, G.W. Huber, W.B. Kim, Electrochemistry Communications 13 (2011) 890–893.
[63] S.M. Choi, M.H. Seo, H.J. Kim, W.B. Kim, Synthetic Metals 161 (2011) 2405–2411.
[64] S. Park, Y. Shao, H. Wan, P.C. Rieke, V.V. Viswanathan, S.A. Towne, L.V. Saraf, J. Liu, Y. Lin, Y. Wang, Electrochemistry Communications 13 (2011) 258–261.
[65] Y. Shao, S. Zhang, C. Wang, Z. Nie, J. Liu, Y. Wang, Y. Lin, Journal of Power Sources 195 (2010) 4600–4605.
[66] J.-J. Shi, G.-H. Yang, J.-J. Zhu, Journal of Materials Chemistry 21 (2011) 7343–7349.
[67] S. Liu, J. Wang, J. Zeng, J. Ou, Z. Li, X. Liu, S. Yang, Journal of Power Sources 195 (2010) 4628–4633.
[68] G. Moon, Y. Park, W. Kim, W. Choi, Carbon 49 (2011) 3454–3462.
[69] L. Wenbo, Z. Dongyuan, Q. Hao, P. Huan, P. Lijia, S. Yi, Chemistry Letters 40 (2011) 104–105.
[70] X.-W. Liu, J.-J. Mao, P.-D. Liu, X.-W. Wei, Carbon 49 (2011) 477–483.
[71] J. Yang, C. Tian, L. Wang, H. Fu, Journal of Materials Chemistry 21 (2011) 3384–3390.
[72] Y. Zhao, L. Zhan, J. Tian, S. Nie, Z. Ning, Electrochimica Acta 56 (2011) 1967–1972.
[73] B. Saner, S.A. Gursel, Y. Yurum, Materials Research Society Symposium Proceedings 1312 (2011) 391–396.
[74] S. Yang, C. Shen, Y. Liang, H. Tong, W. He, X. Shi, X. Zhang, H.-J. Gao, Nanoscale 3 (2011) 3277–3284.
[75] Z. Wen, S. Yang, Y. Liang, W. Heb, H. Tong, L. Hao, X. Zhang, Q. Song, Electrochimica Acta 56 (2010) 139–144.
[76] N. Jha, R.I. Jafri, N. Rajalakshmi, S. Ramaprabhu, International Journal of Hydrogen Energy 36 (2011) 7284–7290.
[77] S.-Y. Yang, K.-H. Chang, Y.-F. Lee, C.-C.M. Ma, C.-C. Hu, Electrochemistry Communications 12 (2010) 1206–1209.
[78] Y.S. Yun, D. Kim, Y. Tak, H.-J. Jin, Synthetic Metals 161 (2011) 2460–2465.
[79] S.H. Lee, N. Kakati, S.H. Jee, J. Maiti, Y.-S. Yoon, Materials Letters 65 (2011) 3281–3284.
[80] E. Yoo, T. Okata, T. Akiat, M. Kohyama, J. Nakamura, I. Honma, Nano Letters 9 (2009) 2255–2259.
[81] Y. Hu, H. Zhang, P. Wu, H. Zhang, B. Zhou, C. Cai, Physical Chemistry Chemical Physics 13 (2011) 4083–4094.
[82] Y.-G. Zhou, J.-J. Chen, F.-B. Wang, Z.H. Sheng, X.-H. Xia, Chemical Communications 46 (2010) 5951–5953.
[83] N. Shang, P. Papakonstantinou, P. Wang, S.R.P. Silva, Journal of Physical Chemistry C 114 (2010) 15837–15841.
[84] L. Feng, G. Gao, P. Huang, X. Wang, C. Zhang, J. Zhang, S. Guo, D. Cui, Nanoscale Research Letters 6 (2011) 551.
[85] R.N. Singh, R. Awasthi, Catalysis Science & Technology 1 (2011) 778–783.
[86] S. Bong, S. Uhm, Y.-R. Kim, J. Lee, H. Kim, Electroctalysis 1 (2010) 139–143.
[87] S. Murugesan, K. Myers, V. Subramanian, ECS Transactions 19 (2009) 249–257.
[88] W.A. Adams, J. Blair, K.R. Bullock, C.L. Gardner, Journal of Power Sources 145 (2005) 55–61.
[89] Y.-X. Li, Z.-D. Wei, Q.-L. Zhao, W. Ding, Q. Zhang, S.-G. Chen, Acta Physico-Chimica Sinica 27 (2011) 858–862.
[90] J. Sato, K. Higurashi, K. Fukuda, W. Sugimoto, Electrochemistry 79 (2011) 337–339.
[91] K. Zhang, Q. Yue, G. Chen, Y. Zhai, L. Wang, H. Wang, J. Zhao, J. Liu, J. Jia, H. Li, Journal of Physical Chemistry C 115 (2011) 379–389.
[92] B. Luo, X. Yan, S. Xu, Q. Xue, Electrochimica Acta 59 (2012) 429–434.
[93] J.-D. Qiu, G.-C. Wang, R.-P. Liang, X.-H. Xia, H.-W. Yu, Journal of Physical Chemistry C 155 (2011) 15639–15645.
[94] S. Wang, X. Wang, S.P. Jiang, Physical Chemistry Chemical Physics 13 (2011) 7187–7195.
[95] S. Zhang, Y. Shao, H.-G. Liao, J. Liu, I.A. Aksay, G. Yin, Y. Lin, Chemistry of Materials 23 (2011) 1079–1081.
[96] Y. Shao, J. Sui, G. Yin, Y. Gao, Applied Catalysis B 79 (2008) 89–99.
[97] M.N. Groves, A.S.W. Chan, C. Malardier-Jugroot, M. Jugroot, Chemical Physics Letters 481 (2009) 214–219.
[98] M.N. Groves, A.S.W. Chan, C. Malardier-Jugroot, M. Jugroot, Tech. Proc. 2009 NSTI Nanotech. Conf., NISTI Nanotech. 3, 2009, pp. 465–468.
[99] G. Kim, S.-H. Jhi, ACS Nano 5 (2011) 805–810.
[100] L.-S. Zhang, X.-Q. Liang, W.-G. Song, Z.-Y. Wu, Physical Chemistry Chemical Physics 12 (2010) 12055–12059.
[101] Y. Xin, J. Liu, X. Jie, W. Liu, F. Liu, Y. Yin, J. Gu, Z. Zou, Electrochimica Acta 60 (2012) 354–358.
[102] M.S. Wietecha, J. Zhu, G. Gao, N. Wang, H. Feng, M.L. Gorring, M.L. Kasner, S. Hou, Journal of Power Sources 198 (2012) 30–35.
[103] H. Li, X. Zhang, H. Pang, C. Huang, J. Chen, Journal of Solid State Electrochemistry 14 (2010) 2267–2274.
[104] E. Antolini, Applied Catalysis B 100 (2010) 413–426.
[105] Y. Chang, G. Han, M. Li, F. Gao, Carbon 49 (2011) 5158–5165.
[106] E. Antolini, E.R. Gonzalez, Solid State Ionics 180 (2009) 746–763.
[107] E. Antolini, E.R. Gonzalez, Electrochimica Acta 56 (2010) 1–14.
[108] E. Antolini, E.R. Gonzalez, Catalysis Today 160 (2011) 28–38.
[109] K.-S. Lee, I.-S. Park, Y.-H. Cho, D.-S. Jung, N. Jung, H.-Y. Park, Y.-E. Sung, Journal of Catalysis 258 (2008) 143–152.
[110] H.L. Pang, X.H. Zhang, X.X. Zhong, B. Liu, X.G. Wei, Y.F. Kuang, J.H. Chen, Journal of Colloid and Interface Science 319 (2008) 193–198.
[111] H.L. Pang, J.P. Lu, J.H. Chen, C.T. Huang, B. Liu, X.H. Zhang, Electrochimica Acta 54 (2009) 2610–2615.
[112] R.S. Hsu, D. Higgins, Z. Chen, Nanotechnology 21 (2010) 165705.
[113] C. Du, M. Chen, X. Cao, G. Yin, P. Shi, Electrochemistry Communications 11 (2009) 496–498.
[114] J. Wu, X.Z. Yuan, J.J. Martin, H. Wang, J. Zhang, J. Shen, S. Wu, W. Merida, Journal of Power Sources 184 (2008) 104–119.
[115] S. Yang, C. Shen, X. Lu, H. Tong, J. Zhu, X. Zhang, H. Gao, Electrochimica Acta 2 (2012) 242–249.
[116] Y. Wang, S. Zhang, H. Chen, H. Li, P. Zhang, Z. Zhang, G. Liang, J. Kong, Electrochemistry Communications 17 (2012) 63–66.
[117] J. Zang, Y. Wang, L. Bian, J. Zhang, F. Meng, Y. Zhao, R. Lu, X. Qu, S. Ren, Carbon 50 (2012) 3032–3038.
[118] B. Seger, P.V. Kamat, Journal of Physical Chemistry C 113 (2009) 7990–7995.
[119] R.I. Jafri, N. Rajalakshmi, S. Ramaprabhu, Journal of Materials Chemistry 20 (2010) 7114–7117.
[120] R. Lv, T. Cui, M.-S. Jun, Q. Zhang, A. Cao, D.S. Su, Z. Zhang, S.-H. Yoon, J. Miyawaki, L. Mochida, F. Kang, Advanced Functional Materials 21 (2011) 999–1006.
[121] R.I. Jafri, T. Arockiados, N. Rajalakshmi, S. Ramaprabhu, Journal of the Electrochemical Society 157 (2010) B874–B879.